2004

FABRICATION AND CHARACTERIZATION OF DETERMINISTIC MICROASPERITIES ON THRUST SURFACES

Sarang Narayan Kortikar
University of Kentucky, sarang@engr.uky.edu

ABSTRACT OF THESIS

FABRICATION AND CHARACTERIZATION OF DETERMINISTIC MICROASPERITIES ON THRUST SURFACES

The deterministic microasperities play a vital role in reducing the coefficient of friction and wear of thrust surfaces and improve the tribological properties of the surfaces. Deterministic microasperities have a specific pattern in terms of size, shape and spacing. These specified geometries are controllable and repeatable. The microasperities are micron scaled asperities and cavities on a surface that form the surface roughness.

The present thesis shows the detailed process to fabricate the deterministic microasperities on thrust surfaces, i.e. stainless substrate, using micro-fabrication processes such as lapping and ultra-violet photolithography in combination with an electroplating (nickel) process. A Novel alignment technique is used to align the photomask with the substrate to get repeatable and aligned patterns on the thrust surface.

Deterministic microasperities are characterized by using precision instruments such as an Optical profilometer, Scanning Electron Microscope (SEM) and Optical microscope to study the various surface parameters such as Average roughness (Ra), Root mean square value (rms) and Peak value (PV) of the thrust surface.

KEYWORDS: Deterministic microasperities, UV Lithography process,
Surface characterization, Novel alignment technique.

Sarang Narayan Kortikar

Date: 11/11/2004

FABRICATION AND CHARACTERIZATION OF DETERMINISTIC MICROASPERITIES ON THRUST SURFACES

By

Sarang Narayan Kortikar

Dr. Lyndon Scott Stephens
(Director of Thesis)

Dr. George Huang
Director of Graduate Studies)
Date: 11/09/2004

RULES FOR THE USE OF THESIS

Unpublished thesis submitted for the Master's degree and deposited in the University of Kentucky Library are as a rule open for inspection, but are to be used only with due regard to the rights of the authors. Bibliographical references may be noted, but quotations or summaries of parts may be published only with the permission of the author, and with the usual scholarly acknowledgements.

Extensive copying or publication of the thesis in whole or in part also requires the consent of the Dean of the Graduate School of the University of Kentucky.

A Library that borrows this thesis for use by its patrons is expected to secure the signature of each user.

THESIS
FABRICATION AND CHARACTERIZATION OF DETERMINISTIC MICROASPERITIES ON THRUST SURFACES

Sarang Narayan Kortikar

The Graduate School

University of Kentucky

2004

FABRICATION AND CHARACTERIZATION OF DETERMINISTIC MICROASPERITIES ON THRUST SURFACES

THESIS

A thesis submitted in partial fulfillment of the requirements
for the degree of Master of Science in the
College of Engineering at the
University of Kentucky

By

Sarang Narayan Kortikar

Lexington, Kentucky

Director: Dr. Lyndon Scott Stephens

(Associate Professor of Mechanical Engineering)

Lexington, Kentucky

2004

MASTER'S THESIS RELEASE

I authorize the University of Kentucky Libraries to reproduce this thesis in whole or in part for the purpose of research.

Signed: Sarang Narayan Kortikar

Date: November 03,2004

To,

My Parents and Family

ACKNOWLEDGEMENTS

I would like to thank the NSF (National Science Foundation) "Surface Engineering and Materials Design Program," Award # CMS-0201445, for sponsoring my present research work. Also, I thank the University of Kentucky for providing an excellent and conducive environment for my research work.

I would like to thank Dr. Scott Stephens, Director of this thesis for his constant support and guidance throughout this research work. I would like to thank him for his valuable inputs, time and insights, which are reflected in the overall quality of this work.

I would like to thank Mark Shaw, Microchem Inc., for giving his valuable inputs in establishing the process, Chris Morgan, Precision Engineering Laboratory, University of Kentucky, for making the alignment marks on substrate and photomask; and Manas Laxmipathy, Zygo Corporation, for helping in the characterization of microasperities.

I would like to thank my friends, roommates and lab mates (Bearing and Seals Laboratory) for their helpful discussion and constant support during my research work.

Finally I would like to thank my parents, sister, brother and brother- in-law who always taught me importance of education in life. I would like to take this opportunity to thank my family for molding me into a successful being. I dedicated this thesis to my family. My sister and brother- in -law stood by me whenever I needed them most.

Table of Contents

ACKNOWLEDGEMENTS iii

List of Tables vii

List of Figures viii

CHAPTER 1 INTRODUCTION 1

1.1 Statement of Problem 2

1.2 Research Objectives 4

1.3 Effect of Deterministic Microasperities on Lubrication 6

1.4 Overview of the Thesis 11

1.5 Literature Review 11

CHAPTER 2 FABRICATION PROCESS 17

2.1 Lithography Origins and History 17

2.1.1 Introduction 18

2.2 Resists used in Lithography 18

2.2.1 Positive Photoresist 18

2.2.2 Negative Photoresist 19

2.3 Deterministic Microasperities 21

2.4 Positive Microasperities 21

2.5 Fabrication Process of Positive Microasperities 22

2.6 Cavities 43

2.6 Fabrication Process of Cavities 44

CHAPTER 3 SURFACE CHARACTERIZATION OF DETERMINISTIC MICROASPERITIES 53

3.1 Nature of Surface 53

3.2 Terminology used in Surface Characterization 55

3.3 Measurement of Surface Roughness 61

3.4 Optical Interferometer 62

3.4.1 Vertical Scanning Coherence Peak Sensing 63

3.5 Results 65

3.6 Surface characterization of Lapped sample without deterministic microasperities 67

3.7 Surface Characterization of Electroplated sample without deterministic microasperities 68

3.8 Surface Characterization of Positive Square microasperities 69

3.9 Surface Characterization of Triangular Positive asperities 71

3.10 Surface Characterization of Square Cavities 73

3.11 Surface Characterization of Triangular Cavities 75

3.12 Electron Microscopy 76

3.12.1 Working Principle of Scanning Electron Microscope 77

3.13 Images Taken From Scanning Electron Microscope 78

3.13.1 Square microasperity 78

3.13.2 Triangular microasperity 80

CHAPTER 4 NOVEL ALIGNEMENT TECHNIQUE 83

4.1 Introduction 83

4.2 Novel Alignment Technique 84

4.3 Working Principle Of Micro EDM 85

4.4 Alignment Marks 87

4.5 Limitation of Novel Alignment Technique.....90

CHAPTER 5 CONCLUSION, DISCUSSION AND 91

FUTURE WORK 91

5.1 Conclusion …… 91

5.2 Discussion 92

5.3 Future Work 94

REFERENCES 95

VITA 97

List of Tables

Table 1 Chart showing the combinations of mask and resist used for.....35

positive microasperities 35

Table 2 Electroplating calculation for Positive asperities.....40

Table 3 Electroplating current calculations for cavities 41

Table 4 Process parameters used during electroplating.....42

Table 5 Chart showing combination of mask and resist used for cavities.....49

Table 6 Processing parameters for fabricating Positive microasperities 51

Table 7 Processing parameters for fabricating Cavities 51

Table 8 Various surface parameters measured during fabrication process.....65

Table 9 Average dimension of microasperities 66

List of Figures

Figure 1.1 Layer diagram of photomask (Square δ2 =0.40) 5
Figure 1.2 Layer diagram of photomask (Triangle δ^2=0.40) 6
Figure 1.3 Determinsitic microasperities (Hexagonal) [9] 8
Figure 1.4 a Full sommerfield pressure distribution over unit cell of positive and negative deterministic microasperities 10
Figure 1.4 b Therotical coefficient of fricition under various condititons……...10
Figure 2.2 Array of triangular positive microasperities (δ^2=0.20).....21
Figure 2.2 Array of square positive microasperities (δ^2=0.40).....22
Figure 2.3 Flowchart for manufacturing of positive micro asperities [9].....23
Figure 2.4 Lapping machine 25
Figure 2.5 Optical flat 27
Figure 2.6 Schematic diagram of electroplating station 30
Figure 2.7 Substrate coated with photoresist using spin coater 32
Figure 2.8 Schematic diagram of fabrication process 33
Figure 2.9a Square positive photomask 34
Figure 2.9b Triangular positive photomask 34
Figure 2.10 Types of exposure and printing methods 35
Figure 2.11 Contact type karl suss mask aligner 37
Figure 2.12 Columns of the photoresist after developing.....38
Figure 2.13 Columns of the photoresist after developing.....38
Figure 2.14a Negative square cavities 43
Figure 2.14b Negative triangular cavities.....43
Figure 2.15 Flowchart for manufacturing of negative asperities [9] 44
Figure 2.16 Schematic diagram of Fabrication process (Negative asperities).....47
Figure 3.1 General topography of solid surface [12].....54
Figure 3.2 Peak [14].....55
Figure 3.3 Valley [14].....56
Figure 3.4 "S"-Average spacing length [14].....56
Figure 3.5 Average roughness value (Ra) [14].....57
Figure 3.6 Average root mean square roughness [14] 58

Figure 3.7.1 Peak value (PV) [14] 59
Figure 3.7.2 Peak value (PV) [14] 59
Figure 3.8 Skewness of surface [14].....60
Figure 3.9 Kurtosis of surface [14].....61
Figure 3.10 3-D Surface profilometer (Zygo Newview 5000®).....64
Figure 3.11 Oblique plot of lapped sample without microasperity 67
Figure 3.12 Surface profile of lapped sample without microasperity.....68
Figure 3.13 Oblique plot of electroplated sample without microasperity 69
Figure 3.14 Surface profile of electroplated sample without microasperity.....69
Figure 3.15 Oblique plot of square microasperity (δ^2 = 0.40).....70
Figure 3.16 Surface plot of square microasperity (δ^2 =0.40).....71
Figure 3.17 Oblique plot of triangular microasperity (δ^2= 0.20).....72
Figure 3.18 Surface plot of triangulalr microasperity (δ^2= 0.20). 73
Figure 3.19 Oblique plot of square cavities (δ^2= 0.40).....73
Figure 3.20 Surface plot square cavities (δ^2= 0.40).....74
Figure 3.21 Oblique plot of triangular cavities (δ^2= 0.20).....75
Figure 3.22 Surface profile plot of triangular cavities (δ^2= 0.20).....76
Figure 3.23 Schematic diagram of working of scanning electron microscope 78
Figure 3.24 Single square microasperity (δ^2 =0.40).....78
Figure 3.25 Edge of square microasperity 79
Figure 3.26 Straightness error in the edge of square microasperity 79
Figure 3.27 Height of square microasperity 80
Figure 3.28 Array of positive square microasperities (δ^2=0.40).....80
Figure 3.29 Triangular positive microasperity (δ^2= 0.20) 81
Figure 3.30 Triangular positive asperity (δ^2 = 0.20) with an edge.....81
Figure 4.1a Layer diagram of photomask square.....83
Figure 4.1a Layer diagram of photomask triangle 84
Figure 4.2 Schematic diagram of working of Micro EDM.....85
Figure 4.3 Actual machining setup 86
Figure 4.4 Actual EDM machining process.....87

Figure 4.5 Cross hairs on substrate 87
Figure 4.6 Cross hairs on photomask 88
Figure 4.7 Aligned patterns after novel alignment technique 88
Figure 4.8 Sqaure aligned patterns (radially arranged) 89
Figure 4.9 Triangular aligned patterns (radially arranged) 89

CHAPTER 1 INTRODUCTION

Tribology is the science and technology of interacting surfaces in relative motion and of related subjects and practices, having its origin in the Greek word 'tribos' meaning rubbing [12]. It is a study of friction, lubrication, and wear with a view to understanding surface interactions in detail and then prescribing improvements in given applications. Understanding the nature of these interactions and solving the technological problems associated with the interfacial phenomenon constitute the essence of tribology. The field of tribology incorporates a number of disciplines, including mechanical engineering, material science and surface physics, as well as a multitude of subjects such as surface characterization, friction, wear, lubrication, bearing materials, lubricants, and the selection and design of lubrication systems. As such, it forms a vital element in engineering.

The importance of friction and wear control cannot be overemphasized for economic reasons and long-term reliability. It is all-important that all designers of mechanical systems use appropriate means to reduce friction and wear through the proper selection of bearings, appropriate lubricants and materials for all interacting surfaces. It is equally important that those involved with manufacturing understanding the tribological origins of unwanted friction, excessive wear, and lubrication failure in their equipment. The lack of consideration of tribological fundamentals in design and manufacturing is responsible for vast economic losses, including shortened life, excessive equipment downtime and large expenditures of energy.

It is estimated that approximately one-third of the world's energy resources in present use appear as friction in one form or another. This represents a staggering loss of the potential power for today's mechanized society. The purpose of research in tribology is understandably the minimization and elimination of unnecessary waste at all the levels of technology where the rubbing of surfaces is involved.

There are new applications that require detailed understanding of the tribological processes on the macro and micro scales. Since early 1980, tribology of magnetic storage has become one of the market places that present new challenges.

Micro Electro Mechanical Systems (MEMS) have begun to appear in the market place with new challenges. Tribology of processing systems such as copiers, scanners and cameras is also important. Along with the industrial advancement in new industrial applications, there has been lots of development in new materials, coatings, and treatments such as synthetic diamond, true diamond and diamond- like carbon films.

The advancement of the tribological application from industrial products, and machinery to the magnetic hard disk and lately in micro/nano applications has not only demonstrated its importance but has also revived interest in this field. With the help of micro fabrication processes such as Ultra-Violet photolithography (UV), micro-electroplating and a lapping process along with the developments in the microscopy processes such optical interferometer and scanning electron microscope, it is possible to produce deterministic microasperities (asperities and cavities) on thrust surface bearing surfaces to improve the overall tribological performance including the reduction in friction, wear, interfacial temperatures, energy consumption and maintenance cost.

1.1 Statement of Problem

Deterministic microasperities on thrust surfaces show significant improvement in overall performance of the thrust surfaces. The deterministic micro asperities have specific size, shape, pattern and orientation. These microasperities have been tested at the actual operating conditions by experimentally changing the various parameters such as applied load, speed of rotation, type of lubrication applied (dry/wet), varying the heights of the microasperities. The results obtained experimentally are compared with analytical models generated by solving the Reynolds equation. Various values such as pressure, coefficient of friction and load carrying capacity are calculated by applying the boundary conditions to the analytical models. These values are compared with the experimental values obtained by testing the thrust surface with microasperities under lubrication conditions in tribometer. There are various micro fabrication processes to produce the microasperities on thrust surface; few of them are list as a) Laser Surface Texturing [LST], b) HARMS LIGA (LIthiographie Galvanoformung Abformung), c) Ultra Violet (UV) Lithography and d) Etching. Each micro fabrication process has certain advantages and disadvantages discussed below.

Etsion [4] developed laser texturing process for fabrication of both positive and negative asperities, but the process is not economical. Later Ronen [9] showed the application of laser textured seals faces in automotive engine. The instantaneous pressure distribution showed that asperity interaction is significant. Area density changes in the range of 5-20% produced in variation of friction force less than 7%. The pore diameter and depth of pores are the critical parameters in overall effect of the lubrication. It is estimated that due to hydrodynamic effects, friction reductions up to 30% could be achieved with laser textured surfaces.

LIGA process has been widely used in the pattern generation in silicon wafer processing but less so in robust applications like surface texturing, lubrication and tribology. The LIGA [6] process used for fabricating positive asperities offers an advantage of achieving higher aspect ratios. LIGA molds are used for fabricating high aspect ratio micro-structures. The accuracy of the patterns produced through the process depends on the quality of mold used in electroplating. The mold produced by lithography process is used to produce plastic sheet PMMA templates. Nickel patterns are produced on thrust surface by electroplating process keeping the template at proximity with the thrust surface. The template can be used several times, but reduce the quality of the micro-structure produced after sometime. The quality of the pattern generated on the surface is depends on template, process conditions of electroplating and contamination. LIGA process is widely used for fabricating HARMS (High Aspect Ratio Microstructures) but can also be used for fabrication of low aspect ratio micro-structures.

Problem Statement

The LIGA process above discussed is an expensive process. LIGA process need "X-ray synchrotron" facility which is available at only 6 stations throughout North America. The LIGA process is suitable for fabricating High Aspect Ratio Microstructures. The above mentioned problem is solved by using modified UV Lithography process discussed in this thesis. UV Lithography stations are less expensive and widely available throughout the world and also process is used to fabricate positive microasperities and cavities with High and Low Aspect ratios.

The modified UV Lithography process developed by Kortikar, S. et al [9] at Bearing and Seals Laboratory at University of Kentucky has been used to fabricate

positive and negative microasperities on thrust surface. The modified UV Lithography process is suitable for fabrication of lower aspect ratio microstructures and also process is economical and extremely useful for mass production. Further, this process is used to fabricate any prescribed cross-section. The surface characterization by using optical interferometer, surface profilometer and SEM images have demonstrated the accuracy and repeatability of microstructures. The accuracy and repeatability of the patterns have significant impact on the hydrodynamic as well as the lubricating properties of the thrust surface.

1.2 Research Objectives

Siripuram [10] did numerical modeling techniques to explore the effects of basic asperity properties comprised of shape, size, concavity and orientation on lubrication characteristics for thrust surface. The results show that, coefficient of friction is largely independent of asperity shape and orientation but sensitive to asperity area fraction (size). The asperity area fraction (size) that minimizes the friction of coefficient is independent of asperity shape and orientation for positive features but dependent on asperity shape and orientation for negative features, however leakage and film thickness are dependent on asperity shape, concavity, orientation and size. For positive microasperities an asperity area fraction of (δ^2_{opt} =0.20) gives minimum coefficient of friction and for a negative asperity (δ^2_{opt} $^{=}$0.80) gives approximate minimum. Their exists a critical value of (δ^2_{cr} $^{=}$0.22), below which the coefficient of friction for a positive asperity is smaller. In contrast to coefficient of friction, leakage rate is quite sensitive to both asperity size (area fraction) and shape (cross section). For a positive asperity, leakage is maximum when δ^2 takes the value of 0.2. This is also value where the coefficient of friction is minimum. In the case of negative asperities, leakage is a maximum when δ^2 is equal to 0.5, as compared to 0.8 for minimum friction coefficient.

The coefficient of friction is independent of the shape of the asperity but sensitive to asperity area fraction; however leakage, load capacity is dependent on the shape and asperity area fraction. Microasperities should have specific shape, size, orientation and spacing between them to improve the tribological properties of thrust surface.

The present scope of thesis to fabricate the deterministic microasperities on thrust surface in figure 1.1, 1.2. The photomask with various asperity shape, size are designed using the results obtained from earlier research work as mentioned above in this chapter. The figure 1.1 shows the layout of the square microasperities and triangular microasperities shown in figure 1.2. The modified Ultra-Violet (UV) photolithography process along with electroplating process is used to fabricate the microasperities on thrust surface. The microasperities can be protrusion (bumps) or recess (holes) in the surface.

The major research objectives are:

a) Design and develop the UV Photolithography process to fabricate the deterministic microasperities on thrust surface.
b) Design the process suitable for producing the positive as well as negative microasperities.
c) Develop the process suitable to fabricate deterministic microasperities of any cross section, shape, size and orientation.
d) Measure the various surface parameters such as surface roughness, skewness, average surface roughness of the deterministic microasperities using optical interferometer and scanning electron microscope.
e) Study the effect of a novel alignment method used in the process on the accuracy and repeatability of the deterministic microasperities.

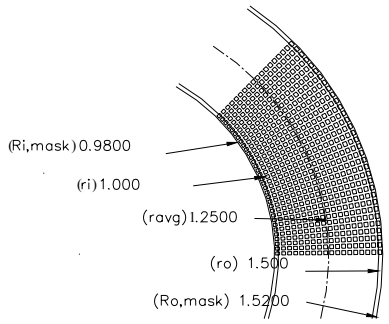

Figure 1.1 Layer diagram of photomask (Square δ2 =0.40)

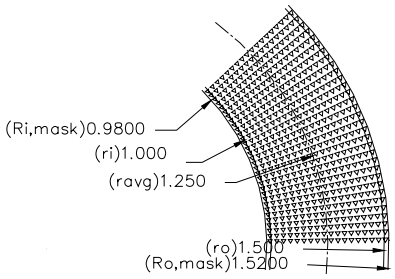

Figure 1.2 Layer diagram of photomask (Triangular δ2 =0.40)

1.3 Effect of Deterministic Microasperities on Lubrication

Lubrication

Surface to surface contact can be prevented by a lubricant, a viscous fluid that can withstand shear loads. Lubrication is the process of introducing such a fluid film to reduce wear and frictional resistance, and also to carry away the heat produced at the interface. Viscosity**,** that represents the internal friction of a fluid, relates the local stresses in a moving fluid to the strain rate of the fluid element. When a fluid is sheared, it begins to move at a strain rate inversely proportional to a property called its coefficient of friction of viscosity, μ, obtained from equation, $\tau = \mu \frac{du}{dy}$ (1)

The above equation shows that relation between shear stress and strain follow a linear relationship, fluid which obey this law are Newtonion fluids and rest of the fluids are Non-Newtonion fluids.

The behavior of sliding surface surfaces is strongly modified with the introduction of a lubricant between them. If we plot, for a journal bearing, coefficient of friction against $\frac{\mu N}{p}$,where μ is the lubricant viscosity, N is shaft speed, and $P = \frac{W}{LD}$

is the specific load. At larger values of $\frac{\mu N}{p}$, the coefficient of friction, is low and is proportional to $\frac{\mu N}{p}$. This is the regime of thick film lubrication. Upon decreasing $\frac{\mu N}{p}$, friction passes through a minimum value, entered into mixed lubrication. For even smaller values of $\frac{\mu N}{p}$,coefficient of friction increases rapidly, marking the complete breakdown of the lubricant film in this so called boundary lubrication regime.

Most of theoretical studies on lubricating films assume that bearing surfaces are smooth. This is a reasonable assumption as long as the thickness [15] of the film separating the two surfaces is significantly larger than the dimensions of the roughness of the surfaces. However, if the film thickness equation is of the order of roughness heights, the smooth film assumption is no longer justified and the roughness effects should be considered.

The local film thickness in a rough bearing consists of the nominal film thickness (h), which is the distance between the mean levels of the two surfaces, and the random roughness amplitudes of the two surfaces. The ratio of the nominal film thickness (h) to standard deviation (σ) of the roughness, h/ σ, is an important parameter indicating the relative importance of roughness effects. When this parameter is large, smooth film theory is sufficiently accurate, but the roughness effects should be considered when this parameter is of the order unity. The regime h/ σ <3 is called the partial lubrication regime due to the presence of interacting asperities (contacts), and the roughness effects are most important in this regime. The regime h/ σ >3 is called hydrodynamic lubrication.

Effect of Deterministic microasperities on Lubrication

The effect of deterministic microasperities on thrust surface is discussed briefly in this section. The deterministic microasperities plays vital role in improving the tribological properties on thrust surface.

To highlight the effect of asperities on hydrodynamic lubrication, consider a slider bearing with the top slider moving with a constant velocity U. Figure 1.3 shows the top and side view and type of cell pattern with a square unit cell and a hexagonal asperity used for this study.

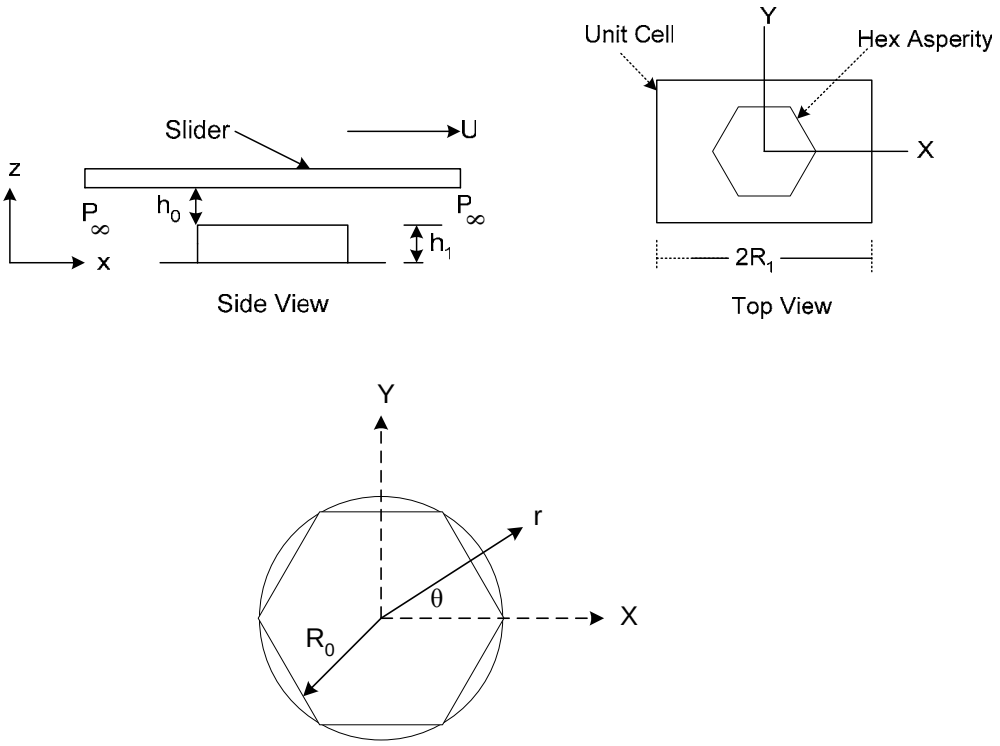

Figure 1.3 Deterministic microasperities (hexagonal) [9]

For a perfectly flat surface, the expression of film thickness (for the case with positive asperity) can be written as

$$h(x,y)=\begin{Bmatrix} h_0 \\ h_0+h_1 \end{Bmatrix} \tag{2}$$

With assumptions stated in reference [8], the governing steady state Reynolds's Equation for pressure distribution along the entire unit cell is given by the Poisson's Equation:

$$\frac{\partial}{\partial x}\left\{h^3\frac{\partial P}{\partial x}\right\}+\frac{\partial}{\partial y}\left\{h^3\frac{\partial P}{\partial y}\right\}=6\mu U\frac{\partial U}{\partial x} \tag{3}$$

For simplicity, the boundary conditions are assumed to be zero between the asperities. Therefore,

$$P(-R_1, y) = P(R_1, y) = 0$$
$$P(x, -R_1) = P(x, R_1) = 0 \quad (4)$$

The resulting pressure distributions over a unit cell for the thrust ring sample geometry for negative asperity under full sommerfeld cavitation condition are exemplified in Figure 1.3. It shows a significant drop on pressure as the lubricant flows through the recess, then an increase when the lubricant escapes the recess. Note that the pressure distribution follows the shape of the hexagonal pattern. For positive asperities, Figure 1.3 will be rotated 180º, because the lubricant will run into a protrusion first, as illustrated in Figure 5.The load support for one unit cell is calculated as per the expression

$$W = \frac{1}{4R_1^{\,2}} \sum_{j=1}^{n} P(x, y) dx dy \quad (5)$$

Coefficient of friction, in case of negative asperities is given as

$$f = \frac{\mu U}{W} \left[\left[\frac{(1 - \partial^2)}{h_0} + \left(\frac{\partial^2}{h_0 + h_1} \right) \right] \right] \quad (6)$$

For full sommerfield cavitation condition, positive and negative pressures will cancel each other, so net load support will be zero. So, for calculation of load and coefficient of friction, a cavitation condition (vaporization of dissolved gas in the lubricating fluid) other than full sommerfeld needs to be introduced during solution process. In this research, Reynolds's cavitation condition is applied by replacing negative pressure with cavitation pressure (zero for simplicity) during each iteration. The result of the calculated friction coefficient under various asperity conditions is presented in Figure 1.4b. It emphasizes the fact that, with proper control over asperity size and pattern, the existence of microasperities will reduce friction coefficient up to 60% [10]. The hexagonal microasperity pattern conducted using UV photolithography process has 1.34 asperities per mm2 and asperity area fraction (™2) of 0.3236. The optimal friction coefficient for this pattern is about 0.25, as is shown with the x mark on Figure 1.4b.

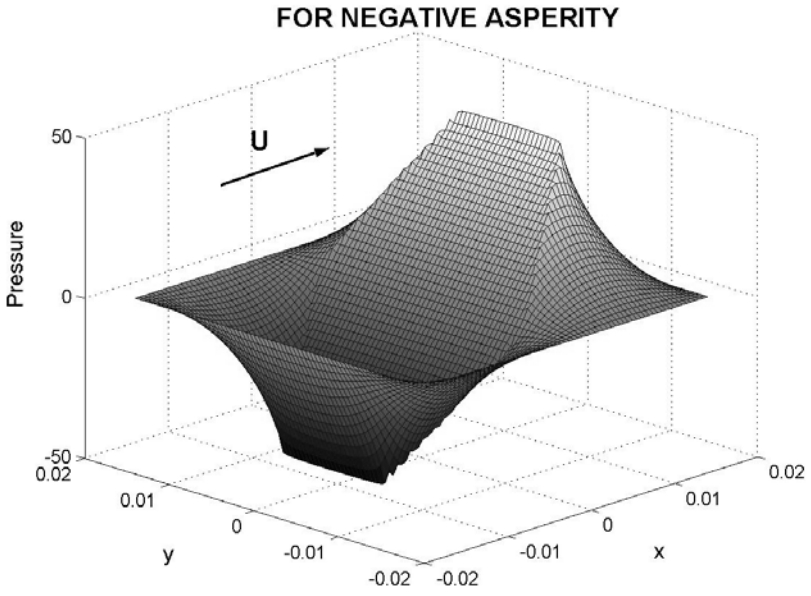

Figure 1.4 a Full sommerfield pressure distribution over unit cell of positive and negative deterministic microasperities [9]

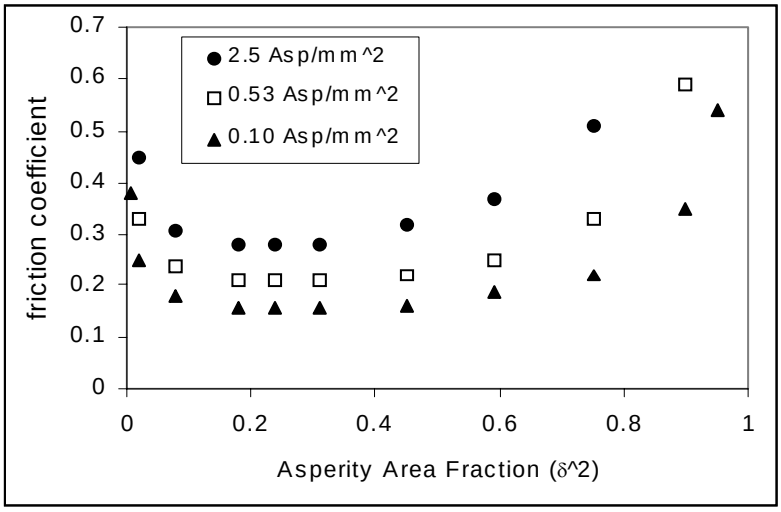

Figure 1.4 b Theoretical coefficient of friction under various conditions [9]

1.4 Overview of the Thesis

The contents of this thesis are described as follows. Chapter 1 gives a theoretical background and the importance of microasperity lubrication. The various fabrication processes used in the manufacturing of the positive and cavities are discussed along with their advantages and disadvantages. Chapter 2 describes the fabrication process to manufacture the positive and negative microasperities. The Photolithography history, origin along with various types of the photoresist used in lithography, including their advantages and disadvantages are discussed in detailed in this chapter. This chapter describes the flow chart and schematic diagram of the modified photolithography as well as nickel plating (electroplating process) developed at University of Kentucky. The various critical parameters affecting the process parameters are discussed. Chapter 3 focuses on the surface characterization of thrust surface by studying the different surface parameters such as Average roughness (Ra), Root mean square value (rms), Peak value (PV), Skewness and Kurtosis of the surface. Dimension of the microasperities using optical microscope and compared with the standard dimension of the photomask.

The various surface parameters measured during the actual fabrication process. The surfaces are characterized using optical microscope, optical profilometer and Scanning Electron Microscope (SEM). By using optical profilometer, average surface roughness (Ra) on the top, within the asperities and at the bottom of the microasperities measured along with the other surface parameters such as predominance of peak or valleys in surface are noted down. Chapter 4 discusses in detail about the novel alignment technique used in alignment of the photomask and substrate in order to produce accurate and repeatable patterns in radial directions. This chapter also discusses the various alignment issues occurred during the process and also discusses the acceptable accuracy of process by using the alignment technique. Chapter 5 discusses in detail conclusions, discussion and the future work in this area.

1.5 Literature Review

The pioneer experimental work in the field of micro-asperity lubrication was observed in the late 60's at Battelle Memorial Institute by Hamilton, D.B., and et.al. [1]. This paper describes a theory of liquid lubrication applicable to parallel surfaces, such as

the surfaces of a rotary-shaft face seal. The lubrication mechanism presented is based on surface micro-irregularities and associated film cavities. Closed- form analytical solutions are obtained giving load capacity as a function of speed, viscosity, and surface asperity dimensions. The theoretical results match significantly with load capacity determined experimentally for three asperity distributions. A lapped carbon graphite stator with 5μin (rms) surface roughness was run against an optically flat transparent rotor. Mineral oil with a kinematic viscosity of 400cst (centistokes) was used as an interfacial film. Narrow, long continuous cavitation streamers were observed.

The interruption in streamers corresponded with the surface roughness of the carbon graphite rotor. Numbers of experiment were carried out in order to study effect of the surface roughness on the cavitation. A smooth, nickel plated rotor was run against a pyrex rotor. Initially, a high amount of torque, but later the torque dropped sown sharply at the end of broadband of cavitation near the inner radius. After some time, cavitation streamers were observed all over the entire surface.

Another set of the experiments was conducted using a flat, but rough stator surface. Roughing was done by lapping a rough stator with 600-grit of the compound. Numerous cavitation streamers were found in both areas. It is extremely difficult to compare the topography of lapped carbon graphite to seal performance because of many microscopic pits and asperities of varying sizes and shapes. Hence, regular patterns were generated on the flat metallic stator surface to facilitate modeling. Using the photo etching technique, cylindrical micro post heights up to 100 μin and flatness on the grooves within 8 μin, this copper ring was soft soldered to a steel substrate and run against smooth pyrex and steel rotors in different experiments. Three different patterns, one varying in asperity diameter and the other in asperity height, were used in this study. Load carrying capacity was found to vary linearly with speed in all these cases. However, the magnitudes were different. Further more, experiments conducted on an identical pattern but with varying heights shows an inverse relationship between load capacity and asperity height.

The author did simple one-dimensional model and it was used to show the association of cavities and asperities. Two-dimensional models, with approximations in boundary conditions, were later used to study the combined effects of asperity geometry

and cavitation. Below experimental critical speeds, no cavitation occurs and hence load support is zero consistent with the theoretical data, within the experimental error. However, the model could not reproduce the pattern of the cavity representation. The experimental values shows, load support were higher, 14.2 psi (0.1 N/mm^2) instead of 7.2 psi (0.05 N/mm^2). The reason attributed for this difference partially, was the assumption of the type of cavities used in theoretical analysis, in which streamers cavitation are not accounted for.

Anno [2] later discussed the micro asperity lubrication distinguishes the classical lubrication theory does not predict the existence of a stable hydrodynamic film for a steady–state, isothermal incompressible flow between smooth and parallel surfaces. The theory given in the paper was developed on this basis by approximate superposition of solutions for pressure distributions corresponding to the flow over circular steps. Load support was predicted to occur in the region behind each asperity and, characteristics of all step-bearing analyses, the theory predicted that sufficiently high finite loads could collapse the film completely. The theoretical model was simplified by approximating the solution as a summation of infinite series and then by truncating the resulting series. A good co-relation between the experimental and theoretical results, both for film thickness and for friction coefficient, was observed.

Anno [3] have compared the load support and leakage performances of positive and negative asperities using the previously mentioned small tilt theory of the asperity tops. They have compared positive square asperities with negative circular asperities, both distributed in a square array. Different arrays (patterns) for micro asperities were also used in this study such as, positive circular asperities in a hexagonal array. Different asperity area fractions such as 0.05, 0.20, and 0.40 are used to study the load support and leakage performance on positive as well as negative asperities. The authors calculated the load capacity and leakage rate for all above mentioned shapes and sizes. The results show, use of microasperities is an effective and controllable technique for obtaining hydrodynamic operation of face seals. All shapes of asperities of comparable dimensions produce similar load support. Negative asperities also produce load support comparable to that of positive asperities. Leakage from micro-asperity lubricated seals generally follows the theoretical predictions, with a modifying influence of rotor angular velocity.

It has been observed that negative asperities were used to obtain load support with negligible leakage.

Etsion [4] have developed an analytical model to predict the relation between the opening force and operating conditions in a mechanical seal with laser textured micro surface structure in the form of microspores. A theoretical model was developed to investigate the performance of laser-textured mechanical seals. Spherical shape pores were analyzed and the average fluid film pressure was calculated. Experimentally it was observed that, the effect of the pore depth over diameter ratio is very significant factor rather than area density of the pores and the radius ratio of seal. The analysis shows that the efficiency of the pores strongly depend on the relation between hydrodynamic effects due to speed, viscosity and seal clearance, and hydrostatic effects due to pressure differential across the sealing dam. A theoretical investigation was complemented by test rig experiments as well as by tests on a water pump in the laboratory and on several pumps in the field. Good quantitative correlation was found between the theoretical model and the test rig experimental results. The water pumps seal showed improved performance with textured faces as compared to original untextured one.

Kligerman [5] did experimental study to evaluate the effectiveness of microstructure, produced by laser texturing, to improve tribological properties of reciprocating automotive components. Good correlation is found with theoretical prediction of friction reduction on a simple test sample. The optimum texture parameters were selected based on the textured parameters such as dimple diameter 100μm, dimple depth 10 μm, and area density 13% resulting in 12 dimples in rows across the 3mm width of each one of the two flat “piston rings”. The optimal values of the texture depend on the operation conditions. It is observed that the texturing reduces the maximum friction force about 30% (from 6.7N to 4.8N), which provide approximately values for un-textured cases as the dimple depth approaches zero. Average values over a full cycle showed up to 40% friction reduction in some cases. The experimental study was performed to evaluate the effect of the laser surface texturing in the form of micro dimples in reciprocating automotive components. Two different specimen configurations, a plain surface and real ring (with micro pores), were tested. Friction reduction up to 40% was found in the first configuration, and up to 30% in the second. Good correlation was obtained with

theoretical results from a model that stimulates the plane surface configuration. Optimum configuration of the laser texturing was in good agreement with theoretical predictions.

The above paper shows the application of laser textured seal faces in improving the overall tribological properties of the seal faces. Approximately 40% total energy is saved by reduction of coefficient of friction. For all the values of depth over diameter ratios, the average friction force diminished as number of asperities was increased. It was estimated that due to hydrodynamic effects, friction reduction up to 30% could be achieved with laser- textured surfaces.

One of the limitations of the laser texturing can produce only negative asperities of spherical and conical shapes. The earlier research shows that, the deterministic asperity with triangular, square and circular shape shows significant improvement in overall tribological properties of the seal faces. There are certain issues (limitations) with laser texturing process such, average asperity depth is 1-30μm, asperity diameter 95-230μm and lowest aspect ratio (0.004-0.3). The asperity manufacturing using laser texturing has issues concerning the heat affected zone and cracking.

The modified LIGA process is an alternate method to fabricate the deterministic microasperities on surfaces. This method is extremely useful for producing positive as well as negative asperities of any arbitrary cross section and orientation, and also able to manufacture asperities with higher aspect ratio.

Later Stephens [6] has proposed the LIGA MEMs manufacturing alternative method, used to pattern the micron sized surface features with arbitrary cross section such (cylindrical, hexagonal, triangular, round) can be fabricated from electroplated nickel, gel cast or plastic. In that paper, LIGA process is used to fabricate a sample thrust bearing surface with hexagonal array of positive asperities (550μm average diameter, 165μm edge-edge spacing and varying heights of 3-100μm). The surface characterization shows the average roughness (Ra) is within 13nm on asperity tops (land). Tribology testing in a non-pressurized oil bath indicates full film conditions and shows a 14-22% reduction in friction coefficient for a thrust surface covered with microasperities. A model confirms the experimental trends and indicates the potential to further reduce the friction coefficient by about 60% through optimization of the asperity geometry and layout.

Zhang, J., [7] in showed the application of a negative photoresist SU8 was tested as an x-ray photoresist in the LIGA fabrication process. SU8 is much more sensitive than PMMA to x-rays and exposure time for SU8 is decreased by a factor few hundred as compared to PMMA, which was aim of the thesis. The detailed LIGA process since, preparation of SU8 samples to the removal of exposed SU8 -embedded in electroplated nickel mold insert is discussed in this thesis. The property of SU8, advantage and disadvantages of SU8 and the various method used to etch the photoresist is discussed in detail in this thesis.

The present thesis briefly discusses the different fabrication process such as LIGA, Laser texturing process to manufacture the deterministic microasperities on the thrust surface. The laser texturing process used to fabricate only cavities on the thrust surface is much faster than conventional LIGA method. Laser texturing has several disadvantages [6] such as a) process is used to fabricate cavities only, b) fabrication of cavities is limited upto spherical and conical shape, c) the average diameter of the pore is in the range of 93μm-250μm, d) the average depth of the pore is up to 10 μm, f) process is suitable for low aspect ratio such as 0.0005-04.

Unlike, laser texturing LIGA process can be used to fabricate both positive asperities and cavities. The alternative fabrication method UV Photolithography is discussed in this thesis overcomes the limitation of laser texturing process and LIGA. The proposed method is economical and shows remarkably accurate patterns. The photo mask can be re-used in this process, and also process is used to fabricate positive asperities and cavities.

CHAPTER 2 - FABRICATION PROCESS

2.1 Lithography Origins and History

Micromachining and microelectronic fabrication starts with lithography, the technique used to transfer copies of a master pattern onto the surface of a solid material, such as a silicon wafer. The origin of lithography process was seen in early 17th Century; Nicephore Niepce while experimenting with various resins in sunlight, managed to copy an etched print on oiled paper by placing it over a glass plate coated with bitumen dissolved by lavender oil. After 2 or 3 hours of sunlight the unshaded areas which remained soluble could be washed away with a mixture of turpentine and lavender oil. By etching a plate, developed by Niepce, in strong acid, the Parisian engraver Lemaitre made an etched copy of an engraving of Cardinal d'Amboise in 1827. The latter copy represents the earliest example of pattern transfer by photolithography and chemical milling. The accuracy of the technique was 0.5 to 1 mm.

The word 'lithography' (Greek for the words 'stone' [lithos] and 'to write' [graphein]) refers to the process invented in 1796 by Alos Senefelder found that stone (he used Bavarian limestone), when properly linked and treated with chemicals, could transfer a carved image onto the paper. Due to chemical treatment of the stone, image and non-image areas became oil-receptive (water- repellent) and oil repellent (water receptive), respectively, attracting link onto the image area and attracting water on non-image areas.

The Niepce process heralded the advent of photolithography [11]. After sometime, photo masking followed by chemical processing lead to the photolithography now used on IC's and micro-machines. The potential application of the photolithography was seen in World War II almost about 100 years after Niepce ad Lemaitre. Interconnections were made by soldering separate electronic components to a pattern of "wires" produced by photo- etching a copper foil laminated to a plastic board. By 1961, methods were devised whereby a photo-etching process produced large numbers of transistors on a thin slice of silicon. Currently the pattern resolution is within 5 micron. Today photolithography and X-ray and charged lithography, submicron accuracy in printing has been achieved.

2.1.1 Introduction

The photolithography process is essentially a pattern transfer process from masks onto a thin film; this process is a combination of accurate alignment and exposing a series of successive pattern, which leads to complex multilayered structures. Photolithography has matured rapidly and constantly improved in its ability to resolve the ever-smaller features. Improvement in higher resolution has impeded the adaptation of alternative, higher resolution lithography techniques such as X-ray lithography.

2.2 Resists used in Lithography

The principal components of the photoresist are a polymer (base resin), a sensitizer and a casting solvent. The polymer changes structure when exposed to radiation; the solvent allows spin application and formation of thin layer on the substrate sensitizers control the photochemical reactions in the polymeric phase. Resists without sensitizers are single-component or one component system. Solvent and other potential additives do not directly relate to the photo activity of resist.

There are mainly two types of photoresist used in the photolithography process:

1) Positive photoresist (e.g. Shipley, PMMA, DQN)
2) Negative photoresist (e.g. SU8 2000, Futurrex)

2.2.1 Positive Photoresist

The photochemical reaction during exposure of a resist typically weakens the polymer by rupture or scission of the main and side polymer chains, and the exposed resist becomes more soluble in developing solutions. The development rate of exposed resist is faster than development rate of unexposed resist.

Most of the positive photoresists are strongly soluble in alkaline solution and develop a mild alkaline. Typically commercially available photoresists are Shipley 1800 series, PMMA (Poly Methylmethacrylate), used for all industrial as well as development purpose. Some common industrial developer for positive resists are Potassium Hydroxide (KOH), an aqueous solution and a surfactant), tetramethylammonium hydroxide (TMAH), ketones, and acetates.

Advantages of Positive photoresist

1) Uniform coating on the substrate
2) Extremely useful for low-aspect ratio microstructures
3) Positive photoresists are less expensive than negative resist
4) Baking conditions are not critical; no cross-linking of polymer is required.
5) The minimum feature size obtained is 0.5 micron or below.
6) The etching (stripping) of the photoresist is extremely easy compared to negative photoresist.
7) It has good thermal stability and residues left after developments are minimal and no swelling of photoresist is observed during developing process.

Disadvantages of Positive photoresist

1) Limited to low aspect ratio only.
2) Less sensitive than negative photoresist
3) Multilayer of the photoresist often create problem such as swelling, non uniform film thickness
4) Adhesion with the substrate is major issue for higher thickness of photoresist.

2.2.2 Negative Photoresist

The photochemical reaction during exposure of a resist typically strengthens the polymer by random cross-linkage of main chains or pendant side chains, becoming less soluble (slower dissolving). The development rate of exposed resist is slower than the development rate of unexposed resist.

Most of the negative resists commercially available are based on free radical initiated photo-cross-linking processes of main or pendant polymer side chains rendering the exposed part insoluble. The insoluble layer forms a “negative” pattern that is used as stencil to delineate many levels of circuitry in semiconductors, and micro-electromechanical systems (MEMS). The insolubility of radiated negative resists can be achieved in one of the two ways: the negative resist material increases the molecular weight through UV exposure (traditional negative resist), or it is photo-chemically transformed to form new insoluble products. The increase in molecular weight is

generally accomplished through photo initiators that generate free radicals or strong acids facilitating polymeric cross-linking or the photopolymerisation of nonnumeric or oligomeric species.

The cross-linking process starts topside, where the light hits the resist first. Consequently, overexposure is needed to render the resist insoluble at the substrate interface. The thicker resist required greater exposure needed for complete polymerization along with large scattered radiation. Scattered radiation at the resist/substrate interface reduced the obtainable resolution. Organic solvent developer swells the cross-linked negative image, further degrading the resolution. To improve the resolution of a negative resist, thinner resist layers can be used; however while using thinner resist, pinholes become problematic. Negative resists are highly resistant to acid and alkaline aqueous solution as well as oxidizing agents. The given thickness of negative resist is more resistant than a corresponding thickness of positive resist. This chemical resistance ensures better retention of resist features even during a long, aggressive wet or dry etch. Negative resists are more sensitive than positive resists but exhibits lower contrast.

Advantages of Negative photoresist

1) Extremely useful for manufacturing of HARMS (High Aspect Ratio Microstructures)
2) Negative photoresists are more sensitive than positive photoresist.
3) Higher thermal stability than positive photoresist
4) Good adhesion to substrate as compared to positive photoresists.
5) Few hundred microns of photoresist can be coated on substrate within single spin coating.

Disadvantages of Negative photoresist

1) Negative photoresists are not economical.
2) Negative photoresists are difficult to etch.
3) Less contrast in developer (ratio of dissolution rate in the unexposed and exposed areas) than positive photoresists.
4) Soft baking and post exposure baking are extremely critical while using negative photoresist.

2.3 Deterministic Microasperities

The microasperities are micron scaled protrusions and recesses formed surface roughness. The protrusions (bumps or post) are called positive asperities and the recesses (holes) are called negative asperities [9]. Deterministic microasperities are surface features having that have specific patterns in terms of shape, size, orientation and spacing in between them. This specified geometry is controllable and repeatable. Figure 2.1 below shows the microasperities fabricated through modified photolithography process developed at "Bearing and Seals Laboratory" at University of Kentucky onto the end face of thrust ring/disc.

This chapter gives the details of the each process steps used in the manufacturing of micro asperities for both positive and negative asperities.

2.4 Positive Microasperities

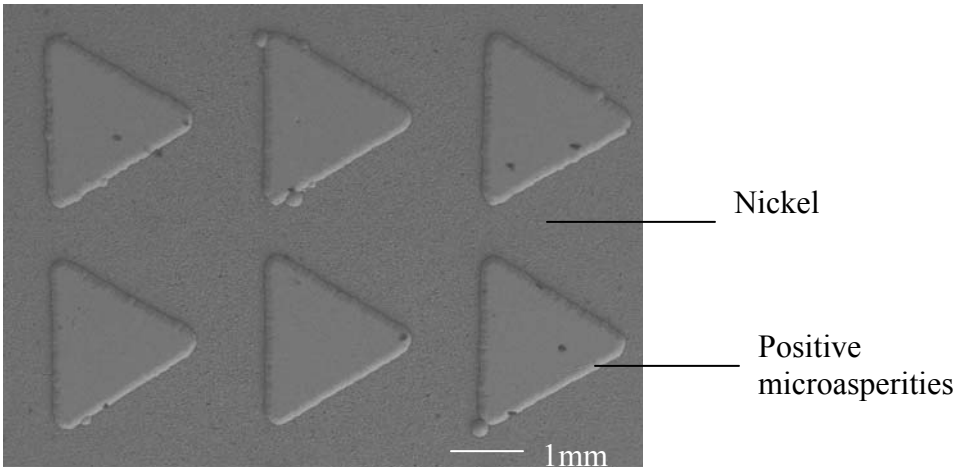

Figure 2.1 Array of triangular positive microasperities (δ^2=0.20)

The above figure shows an array of the microasperities fabricated through the modified photolithography process. The average dimension of the triangle asperities is 470 μm. The microasperities are equally spaced. The average heights of the triangles manufactured were approximately 15 μm. The microasperities are nickel asperities fabricated on the stainless steel (3" Diameter) thrust disk. The accuracy and repeatability

of the patterns based on various processing parameters will be discussed later in this chapter.

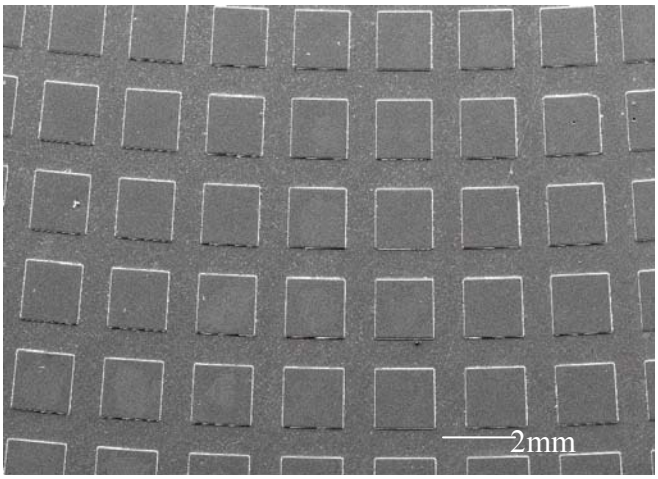

Figure 2.2 Array of square positive microasperities (δ^2=0.40)

The above figure 2.2 shows the SEM image of thrust pad shape microasperities (area fraction ratio (δ^2=0.40). The average dimensions of microasperities are 480x480 microns. The radial spacing and circumferential spacing between the microasperities are 280 micron and 275 micron respectively. The average heights of the microasperities are 15 microns. The microasperities are made of nickel microasperities.

2.5 Fabrication Process of Positive Microasperities

The manufacturing process is the detail step-by-step process to fabricate the positive asperities on thrust surface. The process is broken down into eleven different steps illustrated in following flow chart. The process differs slightly for positive and negative asperities. Adhesive layer and post exposure baking are two extra processing steps in manufacturing of negative asperities. The etching technique for positive and negative photoresist is entirely different processes. Positive photoresists can be easily etched using wet etching and negative photoresist are extremely difficult to etch. Dry etching (Ash burning) process is used for etching the negative photoresists.

The positive and negative asperity uses two different photoresist (a photosensitive material). Combination of photomask and photoresist used we can manufacture either positive or negative photoresist. The table 2.1 [9] shows the various combinations can be

used in the manufacturing process. Shipley 1813® and Microchem SU8- 2050® are positive and negative photoresist respectively used in manufacturing process.

Flowchart for Positive Asperities

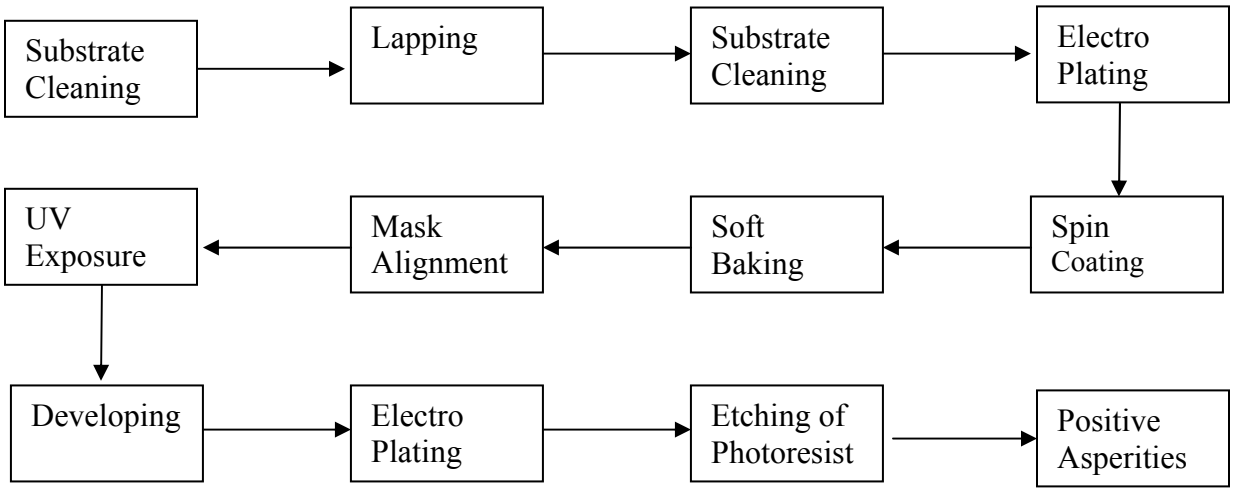

Figure 2.3 Flowchart for manufacturing of positive micro asperities [9]

1) Substrate Cleaning

The first step in modified lithography process used at University of Kentucky is to clean the substrate (Stainless steel ring). The dimension of stainless steel ring is 3" diameter with ¼" thickness. The material of stainless ring is St Steel 304. Following procedure should chemically clean substrate:

Contaminants include solvent stains (methyl alcohol, acetone, isopropyl alcohol, xylene, etc), dust from operators and equipment, and smoke particles. There are several methods for substrate cleaning such as wet treatment, RCA1, RCA2 cleaning procedure with mixtures of hydrogen peroxide with various acids or bases followed by de-ionized water rinses; vapor cleaning; thermal treatment, baking at 1000°C in vacuum or in oxygen. Ultrasonic cleaning helps in removing the dirt and contaminants from the substrate. The prevalent RCA1 and RCA2 wet cleaning procedures are as follows:

RCA1

Add 1 part of Ammonia, (25% aqueous solution) to 5 parts of DI water; heat up to boiling and add 1 part of hydrogen peroxide. Immerse the substrate for 10min. This process removes organic dirt (resist).

RCA2

Add 1 part of hydro-choric acid to 6 parts of de-ionized (DI) water; heat up to boiling and add 1 part of 1 hydrogen peroxide. Immerse the substrate for 10min. This process removes metal ions. The second RCA cleaning process required to keep the oxidation and diffusion furnaces free of metal contamination. Both cleaning processes leave a thin oxide on the substrate.

2) Lapping

The lapping is a metal removal process in precision engineering. The lapping is essentially removes the metal using the hard abrasive material to be used to remove the metal by rotary action of the conditioning ring. The abrasive commonly used is Aluminum oxide mixed in the vehicle slurry in the proportion of 1:8 parts per ounces by weight. Figure 2.4 shows the typical setup for Lapping machine in "Bearings and Seals Laboratory". The surface plate used in lapping is made up of cast iron. The conditioning rings are made up of hard alloy (stainless steel). Each surface plate can accommodate the 3-conditioning rings on the top and the sample (specimen) is placed inside the conditioning ring.

The stress relieving process relieves the stresses/ wrapage induced in the stainless steel substrate after lapping process. It is highly recommended to relieve the stresses induced in order to improve the adhesion of the photoresist with the stainless substrate. The stainless substrate is heating in the oven and the substrate is cooled down in the furnace (annealing process) in order to improve the adhesion of the stainless steel substrate.

The average roughness of the lapped sample is within range of 200-300μm measured by using optical interferometer. The roughness improved by polishing the sample using CMP (Chemical Mechanical Polishing) process. There are certain issues

Figure 2.4 Lapping machine

such as adhesion and bonding on the photoresist on the substrate had been solved by making the surface specifically rough.

The special fixtures are made in order to hold the stainless steel sample. The quality of lapping depends on various parameters such as lapping vehicle, amount of abrasive mixed into the lapping solution, application of pressure on the sample, flow of the liquid on the surface plate while plating. The excessive flow of the slurry may cause hydroplane on the top of surface plate. If the flow of liquid is not enough, it may cause the wear of the surface plate, so the optimum flow of the liquid has to be maintained while lapping.

The application of pressure while lapping is the most critical parameter for the lapping process. The applied pressure is dependent on the surface area of the metal to be lapped. For 3" of stainless steel ring, 16 lb load is applied constantly throughout the lapping process. The stainless steel sample is lapped approximately for 40 minutes. The lapped samples are inspected using the optical flat.

Optical flat is the simple and accurate method to measure the flatness of the surface. The lapped stainless steel sample is placed under monochromatic light source. The optical flat is placed on the top of the lapped sample; the monochromatic light source is turned on. The monochromatic light source will filter the wavelength of white light only and light fringes are observed on the top of the lapped stainless substrate. Most of the mechanical seal applications demand the flatness of the surface within one light band (1 Light Band: 0.0000016") [12]. The nature of the light band will let us know weather the surface has concavity or convexity. The surface is lapped till flatness of the surface is within single light band.

Optical Interferometer (3-D Surface Profilometer) is used to measure the average roughness (Ra) and average root mean square values (rms) of the lapped sample. The flatness of the sample depends on the various processing parameters such as concentration of abrasive used in the solution, lapping vehicle (solution), flatness of the surface plate, flow of the lapping solution during lapping process and application of load on substrate.

Figure 2.5 Optical flat

3) Substrate Cleaning

The substrate is again chemically cleaned using the same RCA1 and RCA2 as explained in earlier in this section to avoid the dirt and contamination on stainless substrate.

4) Electroplating

Electroplating is the deposition of a metallic coating onto an object by putting a negative charge onto the object and immersing it into a solution, which contains a salt of the metal to be deposited. The metallic ions of the salt carry a positive charge and are attracted to the part. When they reach it, the negatively charged part provides the electrons to reduce the positively charged ions to metallic form.

Electroplating process is used to deposit the nickel on the top of the lapped sample. A thin layer of nickel (few microns) is deposited on the top of stainless steel substrate. Figure 2.6 shows, stainless steel substrate acts as cathode and titanium nickel balls acts as anode in this process. The electroplating process is carried out in galvano-static mode keeping voltage constant throughout the process. The current density applied during the process depends on the surface area of the sample to be plated. Normally -0.200mA/cm^2 current density is supplied throughout the electroplating process. The plating solution used in this process is a mixture of nickel sulphamate 450 ml (50% aqueous solution), boric acid (3gram) and water (1000militer). The following chemical reaction is observed during the electroplating process.

$$NiSO_4.6H_2O \rightarrow Ni^{2+} + SO_4{}^{2-} \tag{7}$$

The electroplating bath is made of nickel sulphamate solution and a small amount of boric acid is added into the electroplating bath solution. The bath is heated at constant temperature 55°C. The evaporation of the water is avoided by putting plastic balls on the top of water bath. The pH of the electroplating solution should be maintained constant at 4 through out the plating process. Adding small amount of nickel carbonate in the plating solution can increase the pH, and adding small amount of diluted sulphuric acid in the plating solution can lower the pH of the solution. The plating process is carried out in Galvanostatic mode i.e. keeping the current same through out the process. The plating quality depends on the current density applied during the process and the rate at which

the plating is carried out. The quality of plating depends on various parameters used in process such as maintaining uniform temperature of electroplating bath solution; pH of the solution, current density applied during plating process, plating time and contaminations in the plating solutions. The plating varies according to the amount of nickel deposited on the stainless steel substrate. Initially a thin layer of about 5 microns is deposited on the stainless steel substrate.

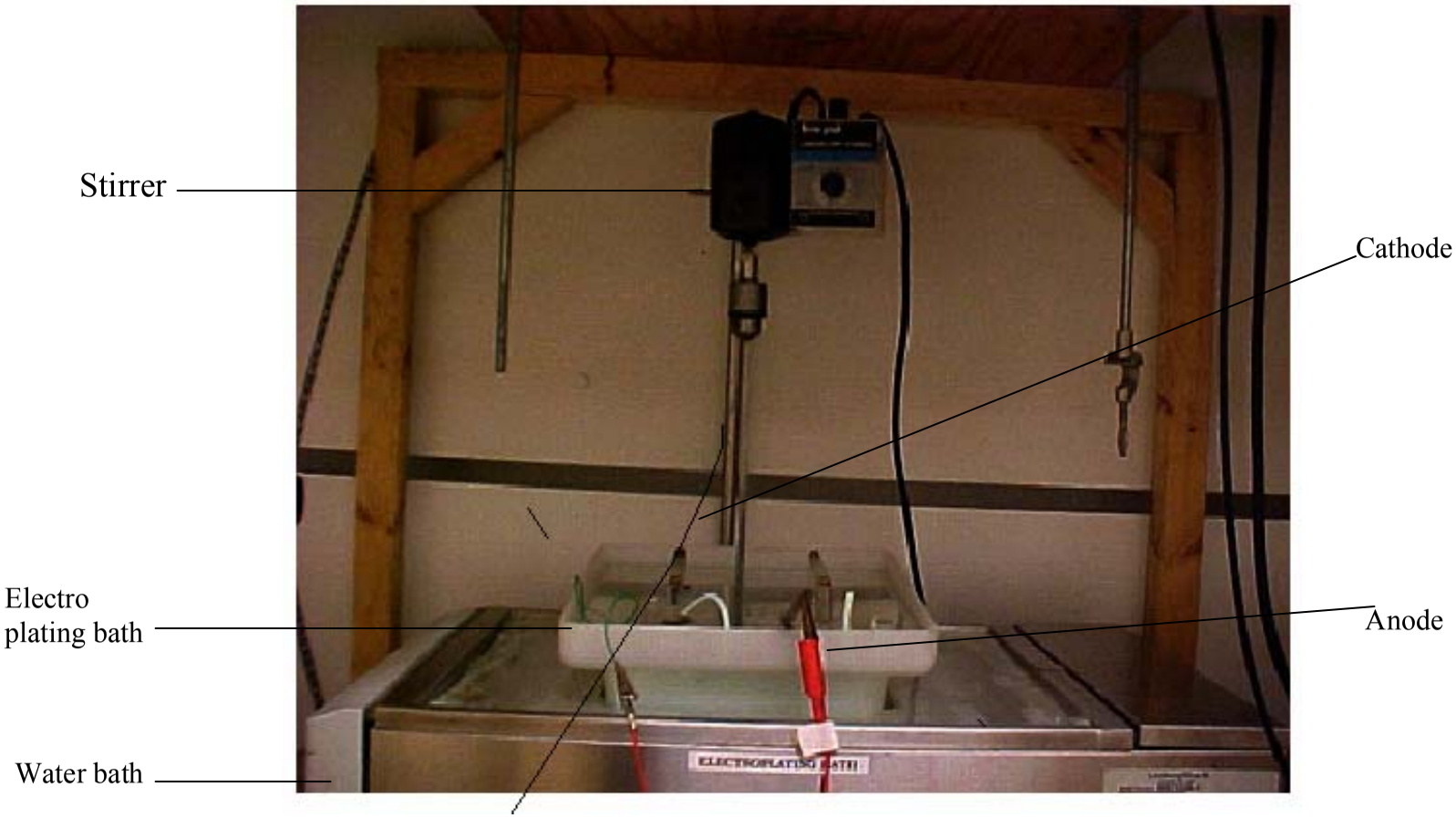

Figure 2.6 Schematic diagram of electroplating station

5) Spin Coating

Photoresist is photo-sensitive material when exposed to ultra-violet light. The types of the photo-resist and their advantages and disadvantages are already discussed at the start of this chapter. The photo-resist used during this process is Shipley 1813®. The photoresist is an organic polymer, sensitive to ultraviolet radiation, deposited on the top of thin layer of nickel. The photoresist is dispensed from a viscous solution of the polymer onto the substrate onto the spin coater. A vacuum chuck holds the substrate in place. The wafer is then spun at high speed depending on the viscosity and the required film thickness to make uniform film. At such high speeds, centrifugal force causes the solution to flow to the edges where it builds up until expelled when the surface tension is exceeded. The photoresist used in this process-Shipley 1813® is spun at a speed of 2000rpm for 30sec. The above equation can be used to predict the thickness of the film that can be spun for various molecular weights and solution concentrations of given photoresist.

The quality of the resist coating determines the density of the defects transferred to the device under construction. The coating thickness of thin glassy resist film depends on the chemical resistance required for image transfer and the fineness of the lines and spaces to be resolved. The application of too much resist results in edge covering or run out, hillocks, and ridges.

The spin coating thickness of the photo-resist used in the process is difficult to measure during the process, the thickness obtained after spin coating the photo-resist is taken from the reference manuals from the photo-resist manufactures. Further more, optimization of the regular photoresist coating process, in terms of resist dispense rate, dispense volume, spin speed, ambient temperature and humidity presents growing challenges in photoresist thickness with of ± 1μm repeatability.

Figure 2.7 Substrate coated with photoresist using spin coater

6) Soft Baking

Soft baking is a process of heating of the spin coated substrate at particular temperature on the hot plate in order to get uniform and stabilized layer of the photo-resist film. After spin coating, the resist still contains up to 15% solvent and may built in stresses. The substrate is therefore pre-baked (soft baked) at 120°C for 3 minutes to remove the solvents and stress and to promote adhesion of the resist layer to the substrate.

Soft baking process also adhere the photoresist layer to substrate. The required thickness of the photoresist used in process is not adequate in single spin coating process; hence multi-layering of the photoresist is done. The photoresist is spin coated on stainless steel substrate and then, resist is soft baked at 120°C for 3 minutes, the resist should be cooled down at room temperature in order to adhere the photoresist layer on top of the substrate. The substrate is again spin coated at 2000rpm for 30sec and a thin layer of photoresist is applied on the substrate again, then substrate is soft baked at 120°C for 3minutes in order to adhere the photoresist layer on top of the substrate. The thickness of the photo-resist obtained by spin coating is measured by using the empirical formula provides in the data sheet of the photo-resist manufacturer.

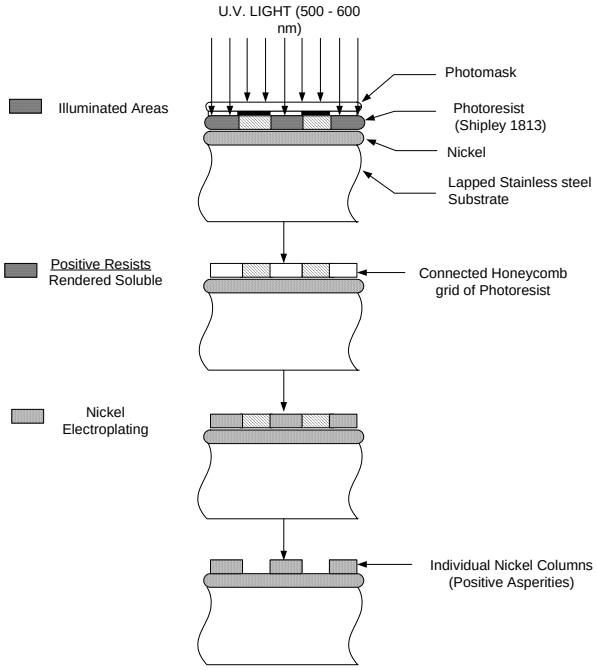

Figure 2.8 Schematic diagram of fabrication process

7) Photomask Alignment

The photoresist-coated substrate is transferred into MJB3 Kurl Suss® exposure system where the photomask and substrate are aligned using precise and accurate stages exposure system. Typically the alignment of photo mask and substrate is critical in generating the accurate and repeatable patterns on the substrate. The alignment marks are made on the photomask and substrate; detailed novel alignment technique is discussed in chapter 4.

Photo mask is typically a square glass plate with the patterns engraved on one side of the photo mask. The accuracy of patterns generated is depends on the accuracy of the patterns engraved on the photo mask. Typical photo mask used in the process is shown as in figure 2.9 a, b. Based on the various combinations of the photomask and photoresist used; we can either manufacture positive or negative asperities. Table 1 shows the various combinations used in process. There are typically two types of photomask mainly positive photomask and negative photomask. Positive photomask is the photomask, where the light passes through the patterns on the photomask. Negative photomask is the photomask, where light passes through the space in between the patterns.

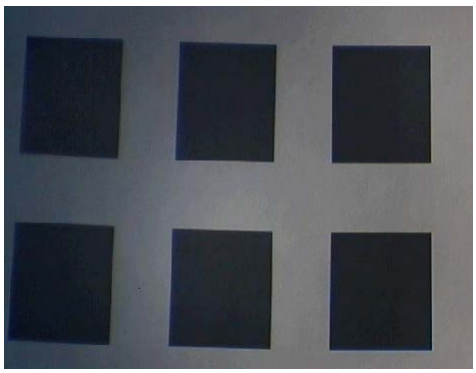

Figure 2.9a Square positive photomask (δ^2 = 0.40)

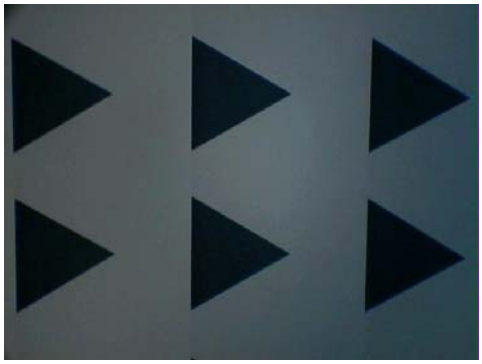

Figure 2.9b Triangular positive Photomask (δ^2 = 0.20)

Figure 2.9a shows the actual image of the photomask (positive) taken through optical microscope. The photomask is made of square type pattern having the area fraction ratio of (δ^2 =0.40). Figure 2.9b, shows the positive photomask with triangular asperities shown by area fraction ratio (δ^2 = 0.20).

Table 1: Chart showing the combinations of mask and resist used for Positive microasperities

Photoresist	Mask Type	After Developing	After Photoresist Etching
Positive*	Positive*	Connected honeycomb grid of photoresist	Individual nickel columns (Positive Asperity)
Positive	Negative	Individual photoresist column	Connected grid of nickel (Negative asperity)
Negative	Negative	Connected honeycomb grid of photoresist	Individual nickel columns (Positive Asperity)
Negative	Positive	Individual photoresist column	Connected grid of nickel (Negative asperity)

8) UV Exposure

Once the photomask has been accurately aligned with the pattern on the stainless steel substrate, the photoresist is exposed through the pattern on the mask with a high intensity ultraviolet light. There are primary exposure methods: contact, proximity and projection. We used Contact type exposure in our process.

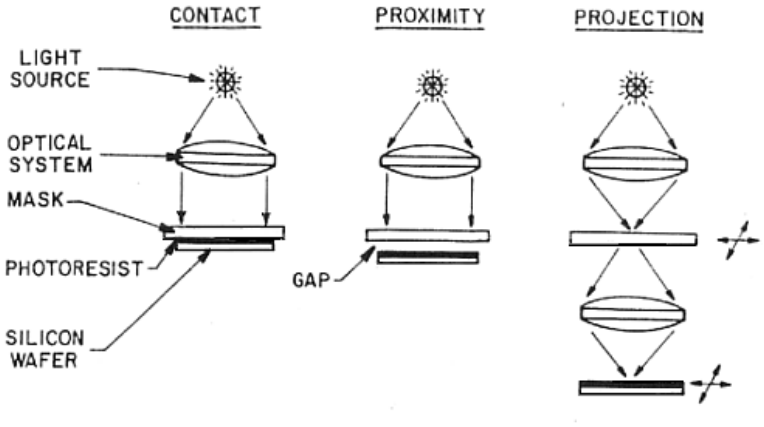

Figure 2.10 Types of exposure and printing methods

Contact Printing

In contact printing, the resist-coated substrate is brought into physical contact with the glass photomask. The substrate is held on vacuum chuck, and the whole assembly rises until the substrate and photomask contact each other. The photoresist is exposed with UV (ultra -violet) light while the substrate is in contact position with the photomask. Because of the contact between the resist and mask, very high resolution is

possible in contact printing. The problem with contact printing is that debris, trapped between the resist and the mask, can damage the photomask and cause defects in the pattern. The contact printing is suitable for small-scale industries and lower resolution work.

Proximity Printing

The proximity exposure method is similar to contact printing except the photomask and substrate are separated by a small gap. This gap minimizes (may not eliminate) mask damage. The approximate gap between the substrate and photomask is about 10-25 micron. The feature resolution obtained is much better than contact printing. Approximately 2-4 micron resolution is possible by proximity printing.

Projection Printing

Projection printing, avoids mask damage entirely. An image of patterns on the mask is projected the resist coated substrate, which is many centimeters away. In order to achieve high resolution, only a small portion of the mask is imaged. This small image field is scanned or stepped over the surface of the substrate. Projection printers that step the mask image over the substrate are called step and repeat systems. Step and repeat projection printers are capable of approximately 1micron resolution.

Exposure

The substrate is placed in close contact with the photomask, and contact-printing method is used. The photoresist is exposed to Ultra-violet light about 500 mj/cm^2 for 30 second. The exposure time and the energy supplied depend on the thickness of photoresist and the resolution of the patterns generated. Too much exposure dose may increase the sidewalls of the features and may damage the geometry of the feature. Too less exposure dose reduces the feature resolution and photoresist remained integral part of the pattern. The optimum dose and exposure time are the critical parameters that affect the overall resolution of the pattern geometry and also accuracy of patterns.

Figure 2.11 Contact type Karl Suss Mask Aligner

9) Development

Development transforms the latent resist image formed during exposure into a relief image which will serve as mask for further subtractive and additive steps. During the development selective dissolution of resist takes place. There are mainly two methods available for development: a) Wet development b) Dry development.

In general, wet development is preferred as compare to dry development process. In our process, we used wet development using MF 319 chemicals for developing the positive photoresist.

Figure 2.12 Columns of the photoresist after developing

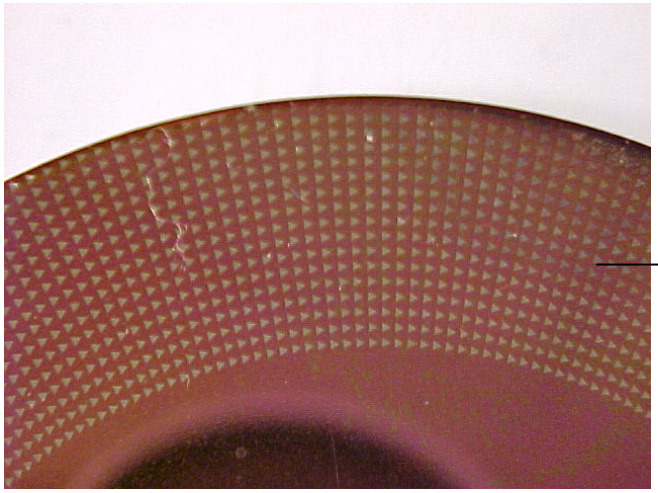

Figure 2.13 Columns of the photoresist after developing

`

Wet development

Wet development by solvents can be based on three different types of exposure – induced changes: variation in molecular weight of polymers (by cross-linking or by chain scission), reactivity change, and polarity change. There are 2 main types of the wet development set-up used a) Immersion & b) Spray developers. During immersion developing, cassette-loaded substrate (wafers) for time period in a bath of developer and batch-immersed for time period in the bath of developer and agitated at a specific temperature.

During spray development, fresh solution is directed across substrate (wafer) surfaces by fan type sprayers. The use of the solvents leads to some swelling of the resist and a loss of adhesion of the resist to the substrate. The wet developing (immersion) method is used for developing the photoresist at the University of Kentucky. Shipley MF-319 is used as developer solution. Substrate is immersed into the developer for 3 minutes. The developing time varies according to the thickness of the photoresist and agitation process. Using de-ionized water and dried using nitrogen gas cleans the photoresist.

Dry development

Dry development used to avoid the use of solvents leads to swelling of resist and loss of adhesion of the resist to the substrate. Dry development is either based on a vapor phase process or plasma. Oxygen- reactive ion etching is used to develop the latent image. The latent image formed during exposure exhibits a difference etches rate to O_2-RIE rather than differential solubility to solvent. Dry development is still in early stages, but ever since there has been awareness for the cleaner environment; dry development has become the need for future.

11) Electroplating

Electroplating process has already been discussed in this chapter. Nickel is deposited in the patterns developed by photolithography process. The plating thickness, rate of plating and amount of current density used in process are process variables. The plating rate varies according to the area to be plated. The plating is carried out in galvanostatic mode. To get the nickel-plating of 15μm, the current density applied is 0.200mA/cm^2. The quality of plating depends on the bath temperature of electroplating

solution, pH of electroplating solution, rate of deposition and the current density applied to substrate. By optimisizing the process parameters smooth layer of the nickel on the top of photoresist. Following chart shows the optimizing for square and triangular microasperities are shown in table below shows the electroplating current calculations for positive and negative micro asperities.

Table 2: Electroplating calculation for Positive asperities

Pattern	Aspect area fraction (δ^2)	Surface area of SS ring (cm^2)	Surface area of asperities (cm^2)	Surface area to be plated (cm^2)	Plating current (Amp)
Square	0.05	45.60	2.6676	2.6646	0.858
	0.40	45.60	10.85	10.85	0.695
	0.70	45.60	18.96	18.96	0.532
Triangle	0.05	45.60	1.28	1.28	0.886
	0.20	45.60	5.37	5.37	0.804
	0.30	45.60	8.10	8.10	0.750

The table 2, above shows the current density calculation for positive microasperities for different asperity area fraction. The surface area of stainless steel ring remains the same for above asperity area fraction but the surface area of the microasperities to be plated varies according to asperity area fraction. In case of the positive microasperities, cavities (holes) are formed after developing process; nickel is filled in the cavities. Hence the surface to be plated is very less as compare to cavities and so the current density.

Table 3: Electroplating current calculations for cavities

Pattern	Aspect area fraction (δ^2)	Surface area SS Ring (cm^2)	Surface area of asperities (cm^2)	Surface area to be plated (cm^2)	Plating current (Amp)
Square	0.05	45.60	2.6676	42.93	0.858
	0.40	45.60	10.85	34.75	0.695
	0.70	45.60	18.96	26.64	0.532
Triangle	0.05	45.60	1.28	44.32	0.886
	0.20	45.60	5.37	40.23	0.804
	0.30	45.60	8.10	37.5	0.750

Table 3, shows the current density calculation for positive microasperities for different asperity area fraction. The surface area of stainless steel ring remains the same for above asperity area fraction but the surface area of the microasperities to be plated varies according to asperity area fraction. In case of the negative microasperities, posts of photoresists are formed and also large amount of cavities formed, the holes to be filled with metal (nickel) by electroplating process. The surface area plated is much more as compare to positive microasperities and therefore the current density supplied to electroplating is much more as compare to positive microasperities.

Table 4: Process parameters used during electroplating

Pattern	Aspect area fraction (δ^2)	pH of solution	Temp of water bath ($^{\circ}C$)
Square	0.05	4.0	55
	0.40	4.0	55
	0.70	4.0	55
Triangle	0.05	4.0	55
	0.20	4.0	55
	0.30	4.0	55

Table 4 shows the various process parameters maintained during the electroplating process such as pH of solution and temperature of water bath.

12) Etching of the Photoresist

The photoresist etching is basically organic polymer etching. The primary consideration is complete removal of the photoresist without damaging the device under construction.

Wet Etching

The wet etching is the process where photoresist is etched by using chemicals. In our process, Acetone used if the post bake is not too long or happens at low temperature, if the temperature is within range of 120° C, acetone can be used. If the post bake temperature exceeds more than 140° C, the resist develops a tough "skin" and has to be burnt away in oxygen plasma. The substrate coated with photoresist is immersed in the beaker contains boiling acetone (120°C); the substrate is heated for 3-4 minutes till the photoresist is entirely removed from the substrate. The substrate is then cleaned with de-ionized water and dried with compressed air and positive asperities are developed on the thrust surface.

2.6 Cavities

The cavities are the micron scaled surface roughness i.e. recesses or holes on the surface. The recent findings on the cavities have generated among the researchers; mainly due to the developments in micro fabrication techniques laser ablation and laser texturing. The earlier work by Etsion, et al; [4] shows that the hemispherical pore diameter manufactured by laser ablation proves to improve the better seal performance and further textured seal carries higher axial load and possesses higher film stiffness. The paper in 1998 dealing with both theoretical and analytical models of spherical shape laser textured seal arranged in radial direction instead of rectangular array. Experimental results show the good correlation with theoretical pressure of average pressure for different seal clearance values.

The process of manufacturing positive asperities is already discussed above in this chapter. Now we will discuss the manufacturing process of negative asperities in detail. The process of manufacturing cavities is almost same as positive asperities.

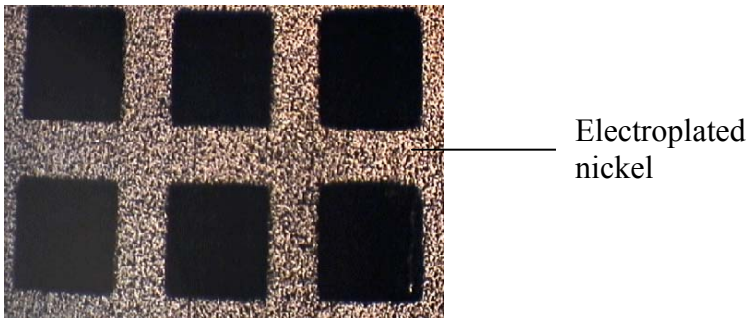

Figure 2.14a Negative square cavities

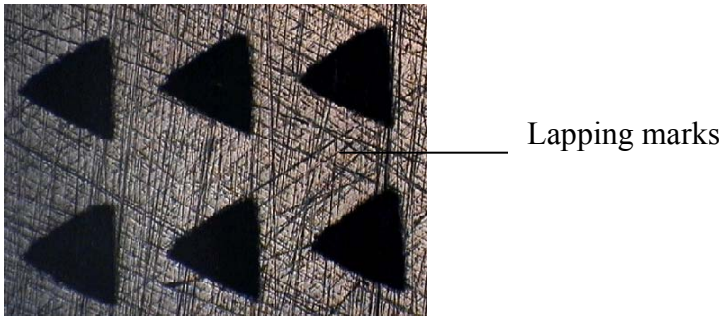

Figure 2.14b Negative triangular cavities

The above surfaces were manufactured at the "University of Kentucky, Bearings and Seals Laboratory" onto the end face of a thrust disc/ring. Figure 2.14a shows the square pattern square micro asperities of 400μm average dimension of side and 25 μm deep. The micro asperities are made up of nickel. Figure 2.14b shows the negative triangular asperities (δ^2 =0.20). Each triangle is an equilateral triangle, the approximate dimension of the side of triangle is 510μm and average height is 450μm. The thrust ring (Stainless ring 1.5" diameter and 1/16" thickness).

2.7 Fabrication Process of Cavities

The process of manufacturing cavities is almost same as positive asperities. The additional steps a) barrier layer b) post exposure baking c) etching of photoresist are mainly different processes compared to the positive photoresist. Higher amount of the exposure dose is needed in order to achieve better resolution of pattern after exposure.
The process of manufacturing is as shown in the flowchart

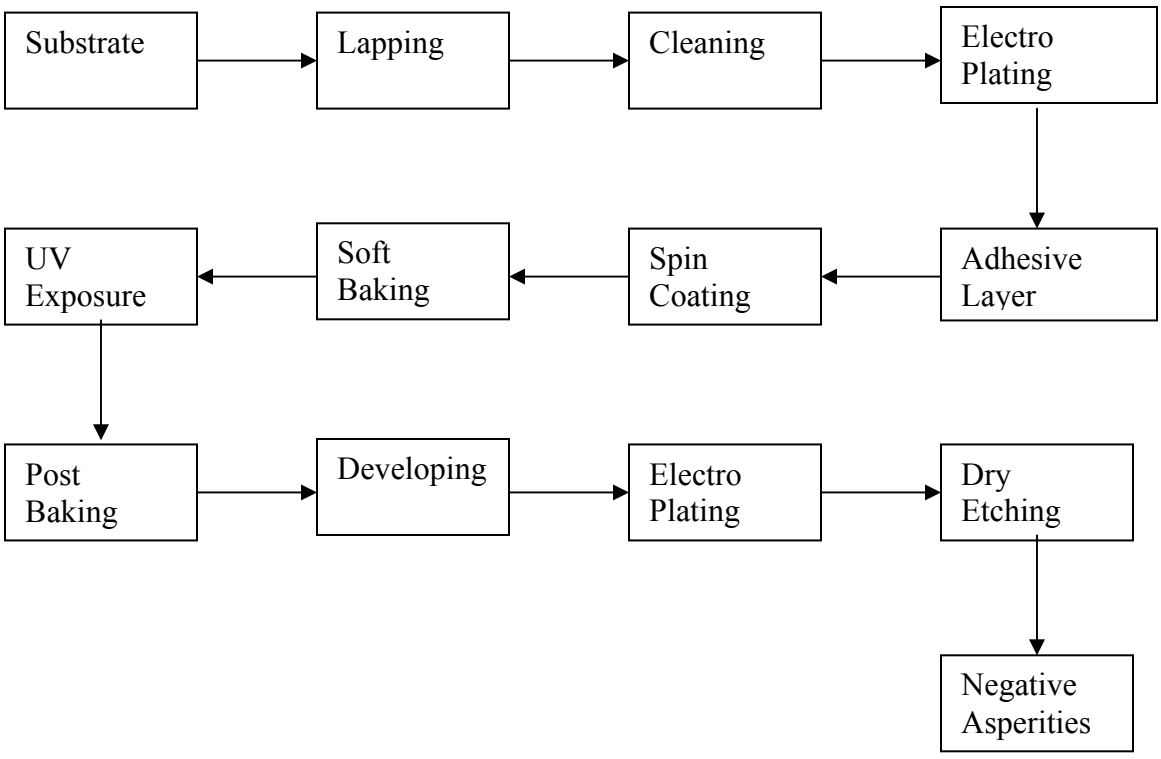

Figure 2.15 Flowchart for manufacturing of negative asperities [9]

The manufacturing process is broken down to 13 process sequences, as shown in the flow chart. The process of manufacturing negative asperities is same as positive asperities except variation in some process sequences such as addition of thin barrier layer, photoresist coating, soft baking and post exposure baking and finally etching process. The schematic diagram of the process is discussed later in this chapter. The etching of the photoresist is difficult as compare to the positive photoresist. The photoresist is used by Dry etching process, ash burning is the process mainly used to etch the SU8 (negative photoresist) by heating the photoresist around 500°C.

1) Substrate Cleaning

Substrate cleaning process is used to remove the organic contamination or dirt associated with the substrate. The cleaning process is similar to the process already discussed for manufacturing positive microasperities. The substrate is cleaned by RCA1 and RCA2 to remove the organic dirt and contamination.

2) Lapping

The chemically cleaned substrate is lapped in order to ensure the flatness of surface within 2 light bands. For normal thrust surface application (i.e. mechanical seal) it is assumed that the flatness of the surface should be within couple of light bands for satisfactory performance of the mechanical seal. The lapping process carried out to ensure the flatness of the surface is similar to the process we have already discussed in this chapter. Ideally the surface should have flatness within 2 light bands measured using optical flat and monochromatic light source.

3) Substrate Cleaning

Substrate cleaning process is used to remove the organic contamination or dirt associated with the substrate. The cleaning process is similar to the process already discussed for manufacturing positive microasperities. The substrate is cleaned by RCA1 and RCA2 to remove the organic dirt and contamination.

4) Electroplating

Electroplating is the deposition of a metallic coating onto an object by putting a negative charge onto the object and immersing it into a solution, which contains a salt of the metal to be deposited. The metallic ions of the salt carry a positive charge and are attracted to the part. When they reach it, the negatively charged part provides the electrons to reduce the positively charged ions to metallic form.

The thin layer of nickel (5μm) is deposited on the top surface of lapped stainless steel sample. The details of the process are already discussed in positive asperities manufacturing. The micro asperities should be deposited on the nickel layer rather than stainless steel surface in order to study the effect of tribological factors on micro asperities. The quality of plating depends on various parameters such as plating solution temperature, pH of solution, plating conditions and plating time.

5) Adhesive layer

The adhesive layer which acts as a barrier layer, normally used to improve the adhesion of photoresist with the substrate, also allowing easy stripping of hard to remove photoresist. Omni coat ® is a polymer used as adhesive layer. The negative photoresist are difficult to adhere to the substrate as compare to positive photoresist. Hence the Omni coat layer is applied on the top of the substrate before spin coating the negative photoresist.

Advantages of Omni coat

1) It is extremely good adhesion promoter, improves the adhesion to difficult substrates like Au, Cu and Quartz.

2) Omni coat can be easily applied by spin coating (i.e. no deposition layer is required).

3) Uses a very thin coating, which minimizes or eliminates under plating.

Omni coat is applied on the electroplated substrate by spin coating process. The electroplated sample is placed on top of spin coater. The substrate is placed in grappling chuck of spin coater. The high vacuum ensures the proper gripping of the substrate on the vacuum chuck. The substrate is spun at angular speed of 3000rpm for 30 seconds, in order to ensure the thin layer of Omni coat on the top of the substrate. The next important step after spin coating is baking of Omni coat®. The omni coated sample is placed on the

hotplate maintained at a temperature of 200°C for 4 minutes. The baking ensures the uniform adhesion of the barrier layer on the top of substrate. The substrate is cooled down at room temperature.

6) Spin Coating

The application of photoresist layer (Microchem SU8-2050®), an organic polymer sensitive to ultraviolet radiation, on top of the adhesive layer. The method to coat the substrate with the photoresist is called spin coating. Spin coating is the most important step to ensure the effectiveness of pattern transfer. This technique ensures the uniformity of the resist layer. The substrate is placed in a grappling chuck of a spinner. The photoresist solution is dispensed on top of the substrate (Microchem SU8-2050®), and then the substrate is spun at the angular speed of 3000 rpm for 30 seconds to obtain 75μm [9] thick photoresist. Such a thickness is necessary to make sure that the desired height of the asperities (10 –50 μm) is achieved after etching and lapping the final substrate.

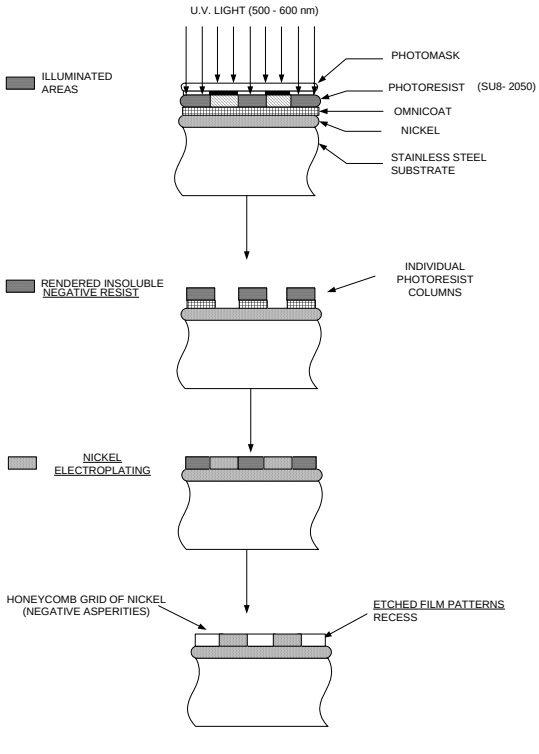

Figure 2.16 Schematic diagram of fabrication process (Cavities)

6) Soft Baking

Soft baking is the process to promote adhesion of the resist layer to the substrate. This process also renders the photoresist coatings photosensitive. The substrate with photoresist is heated at 65°C for 3 minutes and at 95 °C for 7 minutes. Over-soft baking (soft baking the substrate for too long) will degrade the photosensitivity of resists by either reducing the developer solubility or actually destroying a portion of the sensitizer, a photoactive compound. Under-soft baking (soft baking the substrate not long enough) will prevent light from reaching the sensitizer.

7) UV Exposure

The photoresist-coated substrate is transferred into MJB3 Kurl Suss® exposure system in where it is aligned using precise and accurate stages. Typically the alignment of photo mask and substrate is critical in generating the accurate and repeatable patterns on the substrate. The alignment marks are made on the photomask and the substrate; detailed novel alignment technique is discussed in chapter 4. The photomask used in this process is positive photomask (i.e. light will pass through the patterns/ geometries). The following table shows the various combinations of types of photomask and photoresist used in process in order to manufacture either positive or negative asperities.

The photoresist-coated substrate is placed inside a MJB3 Karl Suss® mask aligner to be exposed to UV light. A mask with a desired pattern is placed between the light source and the substrate. There are three methods of exposure: contact, proximity, and projection. The details of the printing method are already discussed before in this chapter. In contact method, the photomask is in physical contact with the photoresist layer, providing very high resolution but also high wear of photomask. The substrate is exposed to UV light with wavelength 500-600 nm for 45 seconds. The exposure time and energy supplied depends on various parameters such as photoresist sensitivity and photoresist thickness. The following table 5 shows, the combination of the photomask and photoresist used in fabricating the cavities.

Table 5: Chart showing combination of mask and resist used for cavities

Photoresist	Mask Type	After Developing	After Etching
Positive	Positive	Connected honeycomb grid of photoresist	Individual nickel columns (Positive Asperity)
Positive	Negative	Individual photoresist column	Connected grid of nickel (Cavities)
Negative	Negative	Connected honeycomb grid of photoresist	Individual nickel columns (Positive Asperity)
Negative *	Positive *	Individual photoresist column	Connected grid of nickel (Cavities)

Note: (*) Combination of Positive photomask and Negative photoresist

9) Post Exposure Baking

The next sequence of photolithography is post exposure baking. This step is desired for cross-linking the photoresist. The substrate is heated at 65°C for 2 minutes and at 95°C for 5 minutes. The cross-linking of polymers helps in improving the resolution of the patterns generated through UV lithography process. The post exposure baking is essential process in manufacturing of negative asperities.

10) Development

After post exposure baking, the substrate is immersed in developer solution. In this process, firstly the substrate is developed using Microchem®SU8–2050 Developer for 7 minutes [9] and then substrate is developed in Microchem® Omni-coat developer for 30sec. developing time may vary depending on the type of photoresist and speed of agitation. Pillars of photoresist for negative asperities are generated at the end of developing process. In order to make sure the photoresist is properly developed in developing solution, the substrate is immersed into the solution of Isopropenol alcohol and agitated for 3minutes. If the solutions turn white in color; it indicates that the photoresist is not yet properly developed. The resist is again immersed into the developer solution till the photoresist is completely developed and the substrate is then cleaned and soaked with distilled water and dried with liquid nitrogen.

11) Electroplating

Electroplating process has been already discussed in this chapter. Nickel is used to fill the patterns developed by photolithography process by electroplating process. The plating thickness, rate of plating and amount of current density used in process are process variables. The plating rate varies according to the area to be plated. The plating is carried out in Galvanostatic mode. To get the nickel-plating of 15μm, the current density applied is 0.200mA/cm^2. The quality of plating depends on the bath temperature of electroplating solution, pH of electroplating solution, rate of deposition and the current density applied to substrate. By optimisizing the process parameter we can able to plate smooth layer of the nickel on the top of photoresist

12) Etching of Negative Photoresist

The most difficult part of the entire process is etching of the photoresist i.e. SU8. Lots of work has been done in this field. Various methods have been proposed, but based on specific application and suitability of process being used. We discuss few methods commonly used for etching of SU8. The process used at University of Kentucky, is Ashing in air/ nitrogen to etch the SU8 photoresist. This is process is explained in detail as below.

Ashing in Air/ Nitrogen

Ashing process is essentially process of heating the photoresist (SU8) in the range of 500°C -600°C in an inert atmosphere. The SU8 is a hydrocarbon polymer, which has strong affinity for oxygen; it reacts with oxygen at elevated temperature and produce carbon dioxide and water. The degree to which SU8 is completely oxidized is function of temperature. At elevated temperatures, the metal mold insert surfaces will be oxidized, which potentially can result in decreasing quality of microstructures. In order to prevent the oxidation of nickel (surface), it is advisable to carry out ashing process in an inert atmosphere such as nitrogen to remove the SU8. It is observed that at higher temperature in range of 500-600°C, SU8 undergoes pyrolysis and some oxidation. At this temperature metal is not exposed to oxygen and therefore, oxidation of mold insert surface is minimized. The removal of the SU8 also acts as annealing steps for the nickel microstructure.

Wet Technique

Sandia National Laboratories has developed two kinds of standard solvent mixtures, Magnastrip and MS-111, which is used to etch exposed SU8. Both solvent systems remove the resists through crazing and peeling rather than dissolution. The main disadvantage of process is not suitable for high aspect ratio features.

A molten salt bath developed at Sandia Lab, an alternative method is a mixture of sodium nitrate and potassium hydroxide operated at 300-350°C and is efficient at completely oxidizing the highly cross linked material with little detectable effect on the Ni parts. The time of removing process is typically less than an hour.

Removal of SU8 molds by Excimer Laser Micromachining

SU8 can be completely removed by scanning the laser beam over the silicon wafer. The laser operation process is carried out smaller size 1.2mm x 0.8mm at flux 0.4 J/cm^2 with 700 shots at a repetition rate of 80Hz. The variation of etch rate with fluence is similar for all the prebake temperatures studied. With an increase in influence temperature, the etch rate increases.

Results

Table 6: Processing parameters for fabricating positive microasperities

Processing parameters				
Substrate flatness	Lapping	-	-	-
Substrate Cleaning	RCA1	RCA2	-	-
Photoresist	Shipley 1813 (Type)	3000Rpm (Speed)	5 sec spread cycle)	30sec (spin speed)
Soft Baking	120º C (2 min)	-	-	-
Exposure	400-500mj/cm2 (Exposure dose)	35sec (duration)	-	-
Development	MF-319 Developer	2-3 min (duration)	-	-
Electroplating	Nickel Deposition	0.200mA/cm2 (current density)	Galavano-Static mode	30mins
Etching	Acetone boiling	120º C	3-4 min	-

The above table 6 shows the actual processing parameters used while fabricating the positive microasperities and cavities. These results are actual findings of this thesis during the research work.

Similarly the process parameters such as photoresist used, spin speed, duration of spinning the photoresist, baking parameters (soft and post exposure baking), exposure dose and development of the photoresist for cavities as shown in the table below.

Table 7: Processing parameters for fabricating cavities

Processing parameters				
Substrate flatness	Lapping	-	-	-
Substrate cleaning	RCA1	RCA2	-	-
Photoresist	Shipley SU8-2050	3000Rpm (Speed)	5 sec (spread cycle)	30sec (spin speed)
Soft baking	65ºC (6 min)	95º C (10min)	-	-
Exposure	400-500mj/cm2 (Exposure dose)	35sec (duration)	-	-
Post exposure Baking	65ºC (2min)	95º C (5min)	-	-
Development	SU8 Developer	5 min (duration)	-	-
Electroplating	Nickel Deposition	0.200mA/cm2 (current density)	Galvano-Static mode	30mins
Etching	Ash Burning	500º C	4-5 hrs.	-

CHAPTER 3 - SURFACE CHARACTERIZATION OF DETERMINISTIC MICROASPERITIES

3.1 Nature of Surface

A solid surface, or exactly a solid –gas or solid –liquid interface, has complex properties depending on the nature of the solids, the method of surface preparation, and the interaction between the surface and the environment. Properties of the solid surface are crucial to surface interaction because the surface properties affect real area of contact, friction, wear, and lubrication.

Solid surfaces, irrespective of their method of formation, contain irregularities or deviations from the prescribed geometrical form. The surface contains irregularities of various orders ranging from shape deviations to irregularities of the order of inter-atomic distances. Ideally no machining process can produce a molecularly flat surface.

Analysis of Surface Texture

Surface texture is the repetitive or random deviation from the nominal surfaces that forms the three-dimensional topography of the surface. The surface texture includes roughness, waviness, lay and flaws.

Micro roughness is formed by fluctuations in the surface of short wavelengths, characterized by hills (asperities) [local maxima] and cavities [local minima] of varying amplitude and spacing. These are large compared to molecular dimensions. The asperities are referred to as peaks in profile (two dimensions) and summits in a surface map (three dimensions). These are considered to include transverse feed marks and other irregularities within the limits of the roughness sampling length. Waviness is the surface irregularity with longer wavelength. Waviness may result due to various factors such as work piece deflection, vibration, chatter, heat treatment, or warping strain. Waviness includes all irregularities whose spacing is greater than the roughness sampling length and less than the waviness sampling length. Lay is the principle direction of the predominant surface pattern, ordinarily determined by the production method. Flaws are unintentional, unexpected, and unwanted interruptions in the texture. In addition, a

surface may contain some gross deviations from nominal shape of very long wavelength, which is known as error of form. They are not normally considered part of surface texture. There is often debate whether the various geometrical features should be assessed together or separately. It is not possible in general to measure all features at the same time. General typology of the solid surface is as shown in Figure 3.1. It is a general classification

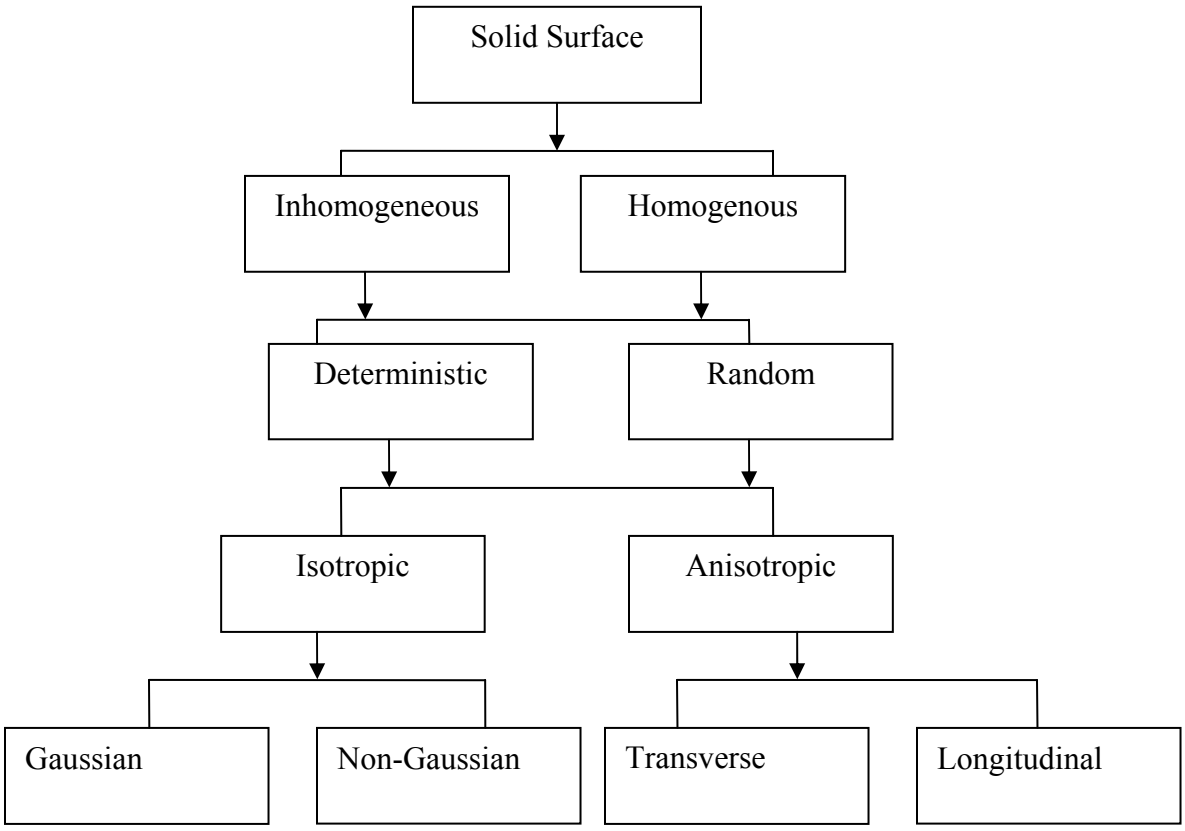

Figure 3.1 General topography of solid surface [12]

Surface textures that are deterministic may be studied by relatively simple analytical and empirical methods; their detailed characterization is straightforward. But the texture of most engineering surfaces is random, either isotropic or anisotropic and either Gaussian or non-Gaussian. The processing method determines whether the surface distribution is isotropic or anisotropic, and either Gaussian or non-Gaussian. Surfaces that are formed by a cumulative process (such as peening, electro polishing, and lapping), in which the final shape of each region is the cumulative result of a large number of random

discrete local events and irrespective of the distribution governing each individual event, will produce a cumulative effect that is governed by Gaussian form. Single-point processes (such as turning and shaping) and extreme- value processes (such as grinding and milling) generally lead to anisotropic and non Gaussian surfaces. The Gaussian (normal) distribution has become one of the mainstays of surface classification.

3.2 Terminology used in Surface Characterization

Peak

Peak is the maximum distance between the center line and the highest peak point within the sample. The center line is defined as the best fit surface selected with the Remove control box. Peak is the value of the highest data point. It is also known as $R_{p.}$

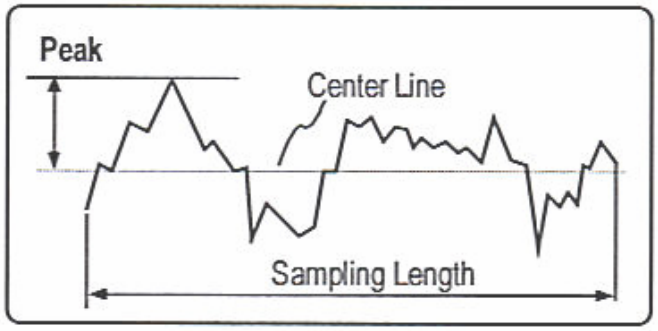

Figure 3.2 Peak [14]

Valley

Valley is the maximum depth between the center line and the lowest valley within the sample. The center line is defined as the best fit surface selected. Valley is the value of the lowest data point. It is also known as Rvc.

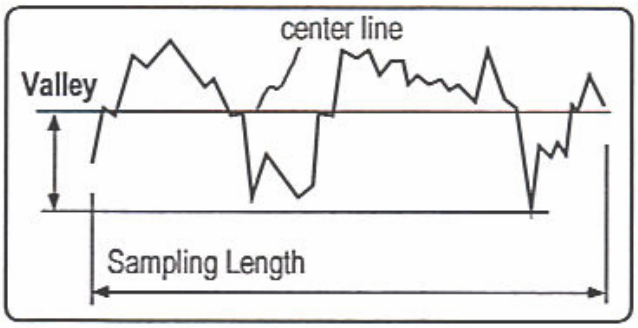

Figure 3.3 Valley [14]

Average sampling length (S)

S is the average spacing between local peaks over the evaluation length. A local peak is the highest point between two adjacent minima. A peak is included only if the vertical distance between the peak and its preceding minima is at least 1% of the R_t the vertical distance from the highest peak to the lowest valley). S is calculated by summing the peak spacing (horizontal distances between the adjacent local peaks) and dividing by the number of peak spacing. If there are three or more consecutive bad data points, the peak spacing is not included.

In the example above, S is calculated from six peak spacing. Note that peak 3 and peak 5 are not used in the peak spacing because the vertical distance from their preceding minima are less than 1% Rt. Peak 8 is neglected because of bad data points before its seceding peak. S for the above example is calculated by:

$$S = \frac{s_1 + s_2 + s_3 + s_4 + s_5 + s_6}{6} \tag{8}$$

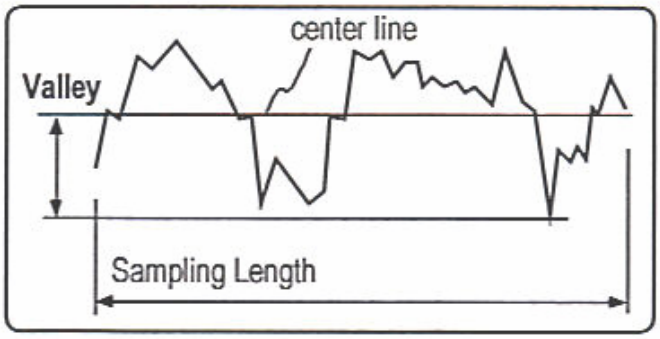

Figure 3.4 “S”-Average spacing length [14]

Points

Displays the number of valid data points in a particular data set. Also known as pixels, or the number of camera pixels used in the measurement and/or analysis. The number of data points can vary due to the use of masks, data dropout, and the instrument components.

Average roughness (R_a)

R_a is the arithmetic average deviation from the enter line. The centerline is defined as the best fit surface selected with the Remove control. Since Ra is a roughness parameter, surface figure should be removed from the data with the Remove control for this result to be meaningful.

$$R_a = \frac{y_1 + y_2 + y_3 + ... + y_n}{N} \tag{9}$$

Where y_x is the absolute value of each point and N is the number of discrete elements.

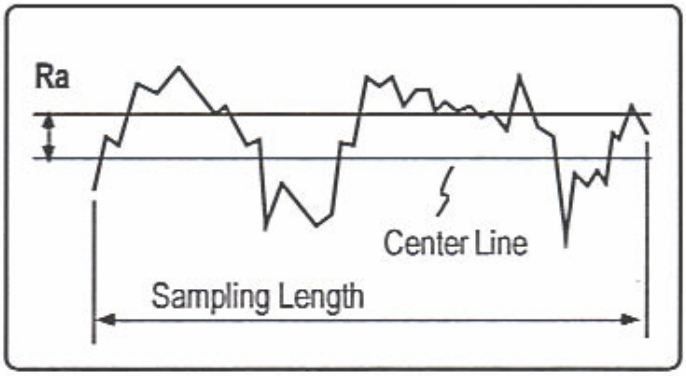

Figure 3.5 Average Roughness value (Ra) [14]

Root mean square (rms)

Root mean square or rms is the root-mean square deviation from the center line. This is a method of calculating an average by squaring each value and then taking the square root of the mean. The center line is defined as the best fit surface selected with the remove control. It is also known as R_q.

The rms result is calculated as the standard deviation of the height (or depth) of the test surface relative to the reference at all data points in the data set. Since rms is a

roughness parameter, surface figure should be removed from the data with the Remove control for this result to be meaningful.

The rms result is the root-mean-square of surface figure error or transmitted error relative to a reference surface. The rms result is an area weighted statistic; when used for optical components, it more accurately depicts the optical performance of the surface being measured than the PV statistic because it uses all the data in the calculation.

$$rms = \left(\frac{y_1^{\,2} + y_2^{\,2} + y_3^{\,2} + ... + y_n^{\,2}}{N} \right)^{0.5} \tag{10}$$

Where: Y_x are the height elements along the profile and N is the number of discrete points

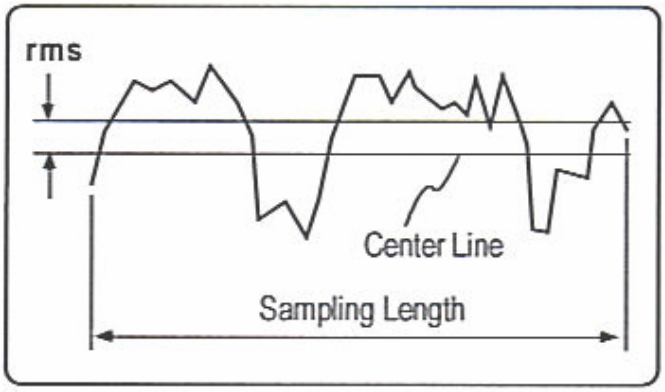

Figure 3.6 Average root mean square roughnesses [14]

Peak value (PV)

PV (Peak-to-Valley) is the distance between the highest and lowest points within the sample. PV is also known as R_t. When used to quantify roughness, PV is the maximum roughness height. PV is the worst case point-to-point error in the data set. PV compares the two most extreme points on the surface; thus, it is possible for two very different surfaces to have the same PV value. This figure illustrates that different surfaces can have the same PV; three surfaces are superimposed over the top of each other.

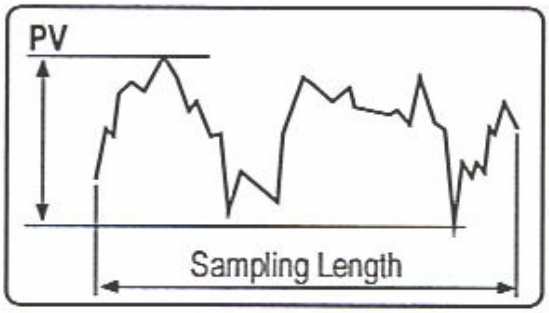

Figure 3.7.1 Peak value (PV) [14]

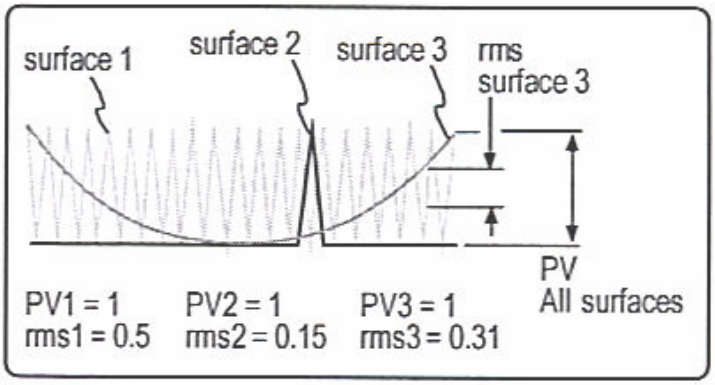

Figure 3.7.2 Peak Value (PV) [14]

R_{sk} (Skewness)

R_{sk} or skewness is a measure of the symmetry of the profile about the center line. It will distinguish between asymmetrical profiles of the same R_a and rms.

$$Rsk = \frac{1}{n(R_q)^3}\sum_{i=1}^{j=1}(Y_i)^3 \qquad (11)$$

Where n is the number of data points Y_i in the profile and R_q is the root-mean-square roughness. Negative skewness, often specified from -1.6 to -2.0, is used as a criterion for a good bearing surface. Positive skew is sometimes specified for electrical contacts.

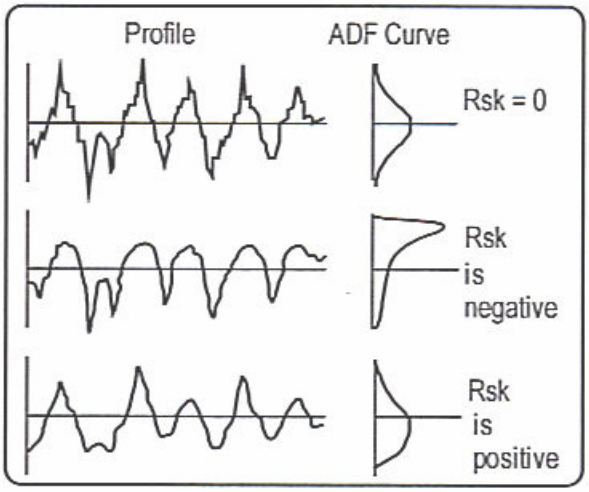

Figure 3.8 Skewness of surface [14]

R_{ku} (Kurtosis)

R_{ku} or Kurtosis is the measure of the sharpness of the ADF (Amplitude Density Function) curve and of the "spikiness" of a surface. Spikiness does not necessarily mean the sharpness of individual peaks and valleys. The sharper the ADF curve, the greater the value. Kurtosis values can range from 0 to 8.

$$Rku = \frac{1}{n(R_q)^4}\sum_{i=1}^{j=n}(Y_i)^4 \tag{12}$$

Where n is the number of elements Y_i in the profile and R_q is the root-mean-square roughness. Kurtosis is also a measure of the randomness of profile heights: a perfectly random surface has a kurtosis of 3; the less random and more repetitive the surface, the further the kurtosis value is from 3. Kurtosis is sometimes specified for the control of stress fracture.

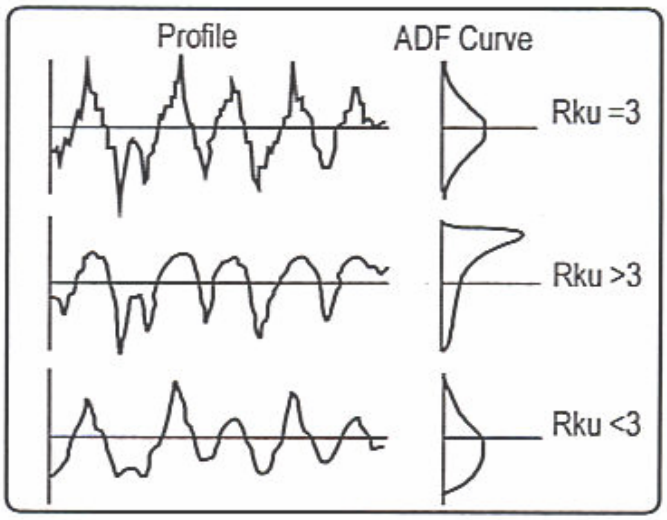

Figure 3.9 Kurtosis of surface [14]

3.3 Measurement of Surface Roughness

The surface characterization of micro asperities is done in order to study the various surface parameters such as average surface roughness (R_a), root mean square (rms) value, surface roughness on top of microasperities and roughness in between the asperities, tilt in the micro asperities, and skewness of the surface. The previous study shows that the surface parameters play a vital role in the performance of thrust surfaces. The tribological and lubricating properties of the surface are main the interests of study in this thesis. There are various precise instruments available for roughness measurement. The measurement technique can be divided into two broad categories a) Contact Type and b) Non Contact type.

A contact type component actually contacts the surface during actual measurement. A contact type instrument actually damages surfaces when used with a sharp stylus tip, particularly soft surfaces. For these measurements, the normal loads have to be below enough so that the contact stress does not exceed the hardness of the surface to be measured. Taylor Hobson is a contact type instrument that uses electric amplification. The stylus technique recommended by ISO is generally used for reference purposes.

In Non-contact type measurements are done without actually making contact with the surface. It is a non-destructive type of roughness measurement technique. An optical

interferometer is an example of a non-contact type roughness measurement. The optical interferometer can be used to measure the surface roughness with lateral resolution ranging from microscopic to atomic force. This instrument is widely used in research to measure roughness with extremely high lateral resolution, i.e., nanoscale roughness.

There exist a different number of techniques based on application and physical principle involved. a) Mechanical stylus method b) Optical stylus method c) Scanning probe microscopy (SPM) methods d) Fluid methods e) Electrical methods and f) Electron microscopy methods. We will discuss the Optical stylus method in details, since we use the Optical interferometer to measure the surface characteristics of the micro asperities.

Optical Method

When electromagnetic radiation (light wave) is incident on an engineering surface, it is reflected either specularly or diffusively or both. Reflection is totally specular when an angle of reflection is equal to the angle of incidence (Snell's law); this is true for perfect smooth surface. Reflection is scattered when the energy in the incident beam is distributed as the cosine angle of reflection. As roughness increases, intensity of specular beam decreases while the diffracted radiation increases in intensity and becomes more diffused. In most real surfaces, reflection are neither completely specular nor completely diffuses. This clearly shows the relationship between the wavelength of radiation and the surface roughness will affect the physics of reflection; thus a surface that is smooth to radiation of one wavelength may behave as if it were rough radiation of a different wavelength.

3.4 Optical Interferometer

Optical interferometry is a valuable technique for measuring surface roughness on both a macroscopic and microscopic scale. The traditional technique involves looking at interference fringes and determining how much they depart from being straight and equally spaced. The reflected beam from two parallel plates placed normal to the incident beam interfere and the result is the formation of fringes. The fringe spacing is a function of the spacing of the two plates. If one of the plates is a reference plate and another is an engineering surface whose roughness is to be measured, the fringe spacing can be related

to surface roughness. This is the typical principle of a two- beam optical interferometer. The same principle is used in most optical interferometers. With suitable computer analysis, these can be used to characterize a surface completely. The most common method for the quantitative measurement of surface roughness is to use a two- beam interferometer.

The actual sample can be measured directly without applying a high reflective coating. The surface- height profile itself is measured. The option of changing the magnification can be used to obtain the different values of lateral resolution and different fields of view. Short wavelength visible- light interferometry and computerized phase shifting techniques can measure the surface height variations with resolution better than 1/100 of wavelength of light. The short wavelength of visible light is a disadvantage, however, when measuring large surface height variation and slopes.

3.4.1 Vertical Scanning Coherence Peak Sensing

Several precise instruments such as an Optical microscope, an Optical interferometer (3-D Surface profilometer) and a Scanning Electron Microscope (SEM) are used for characterizing the micro asperities manufactured using modified lithography process.

Figure 3.10 Surface Profilometer [Zygo Newview 5000]

3.5 Results

The surface characterization of micro asperities is done in order to study the various surface parameters such as average surface roughness (R_a), root mean square (rms) value, surface roughness on top of micro asperities and roughness in between the asperities, tilt in the micro asperities, and skewness of the surface. The average value of the flatness measured by using the optical flat. The flatness of the substrate affects the overall the tilt and height of the microasperities on the stainless substrate. The previous study shows that the surface parameters play a vital role in the performance of thrust surfaces. The tribological and lubricating properties of the surface are main the interests of study in this thesis.

The thrust samples fabricated by using photolithography and electroplating process are characterized using the optical microscope and surface interferometer. 3 different samples of each area fraction ratio are fabricated using the process. The measurement of the samples is taken during each processing steps. The various process parameters used in the fabrication process are also recorded in the charts as shown below.

Table 8: Various surface parameters measured during fabrication process

Pattern	Area of Fraction (□ ..)	Ra (before plating After lapping) (μm)	Ra (After lapping and After plating) (μm)	Ra (Avg. roughness) (μm) on top of microasperities	rms (root mean square) (μm) on top of microasperities	PV (peak value) (μm) over the entire surface
Square	(*)0.40	0.160	0.300	0.250	0.225	14.375
	0.40	0.200	0.325	0.425	0.240	15.036
	0.40	0.155	0.330	0.325	0.230	14.750
Triangle	(#)0.20	0.170	0.330	0.190	0.150	9.870
	0.20	0.165	0.340	0.185	0.175	10.790
	0.20	0.225	0.350	0.180	0.160	11.050

(*) The measurement of the square positive microasperities is shown below. The three different measurements are taken of three different samples during the surface characterization process. The measurements are taken at each different process steps

during entire fabrication process. The average roughness (After lapping but before nickel plating) is recording and then a smooth layer of nickel is deposited on top of the thrust surface, after depositing a smooth layer, again average roughness value is measured. The microasperities are fabricated on the top of nickel plated stainless steel sample and the average roughness value on the top of the microasperities as well as root mean square value is recorded. The peak value will give fair idea about the surface variation within the surface. The higher the peak value, higher the hills and valleys on the surface. Similar measurements are done for triangular microasperities. The height of the microasperities can be controlled by lapping the microasperities to the specified heights.

Table 9: Average dimension of microasperities

Pattern	Area of Fraction (□)	Average. dimension of asperity (Side µm)	Average Height (µm)	Radial distance between two asperity (µm)	Circumferential distance between two asperities (µm)
Square	0.40	479x479	15	284	275
	0.40	487x487	16	280	280
	0.40	475x475	16	282	268
Triangle	0.20	515	15	248	746
	0.20	519	17	245	750
	0.20	510	16	251	751

The above table shows the actual dimension of the fabricated microasperities using the optical microscope. Three different measurement of each thrust surface is taken to ensure the repeatability within the measurement. The "z" axis of optical microscope is used to measure the thickness (height) of the microasperities as well as depth of the microasperities. The "x" and "y" axis used to calculate the lateral dimension of the microasperities.

The dimensions measured are compared with the dimensions of the photomask. The average dimensions of square (δ^2=0.40) from photomask are 480x480 µm side, radial and circumferential dimensions are 280, 275 respectively. The actual measured dimensions for square microasperities are in range of 475-487 µm, i.e. the average variation in the dimension (sides of microasperities) is within the range of 2% variation with respect to the standard dimension, average variation in the dimension in the variation of radial and circumferential dimension is within range of 0.5% and average

deviation for the height of microasperities observed with range of 0.25% of standard dimension. Similar measurements observed for triangular microasperities.

3.6 Surface characterization of Lapped Sample without deterministic microasperities

The surface roughness and flatness are the important parameters in the overall manufacturing of the microasperities. During the manufacturing step, the thrust surface is lapped in order to get uniform flatness.

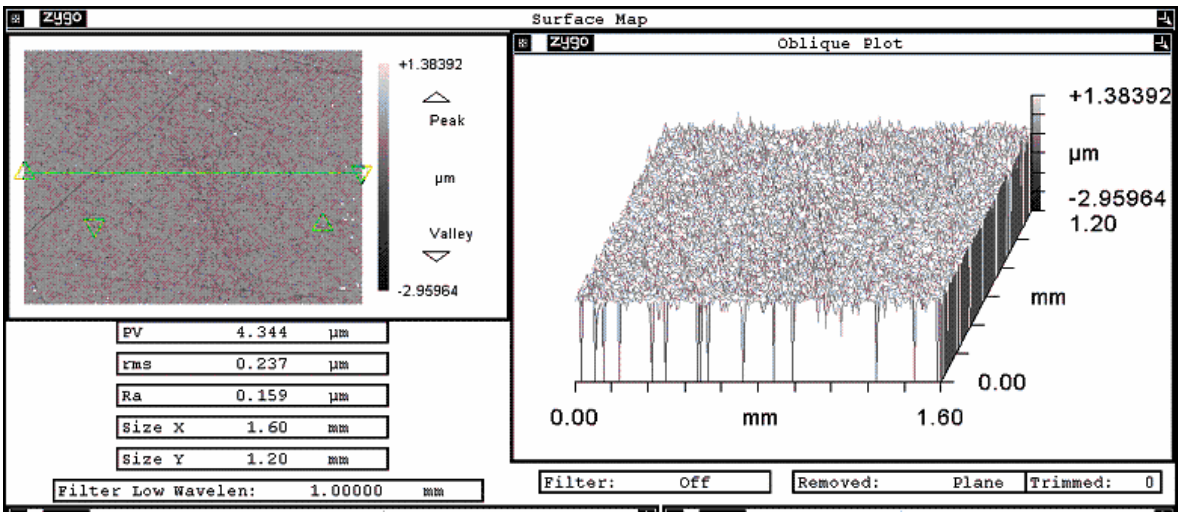

Figure 3.11 Oblique plot of the lapped sample without microasperity (*)

Figure 3.11 shows the measurement of the surface using the 3-D surface profilometer. The Oblique plot is a three dimensional display of the data with the 'x'-axis horizontal, the 'y'-axis inclined to the horizontal, and the 'z' axis vertical. All the axes of the plot typically include the labeled scales. The average roughness (R_a) of the surface is noted (0.169µm). This roughness value is the average of the data points taken across the entire surface. The lower the R_a value, the better the surface flatness. The PV (Peak Value) is an indication of the amount of the peaks and valleys present in the surface. The lower the PV (4.291µm) value, the lower the variation in the surface profiles. The average root mean square (rms: 0.249µm) value indicates the mean square average roughness value over the entire surface; the lower the Rms value, the better the surface profile and overall flatness of the surface. The Size "X" is the dimension of the data set in

the x-axis of the Video monitor screen and similarly Size "Y" is the dimension of the data set in the y-axis of the Video monitor screen.

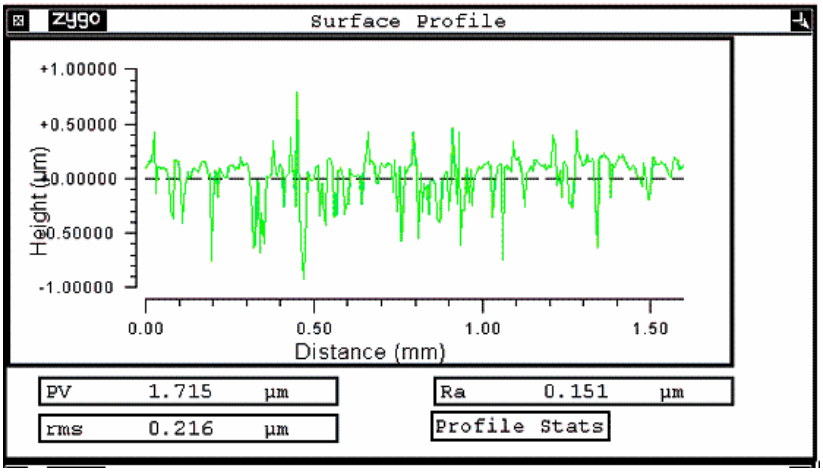

Figure 3.12 Surface profile of the lapped sample without microasperity (*)

Figure 3.12 shows the surface profile plot of the lapped surface. The x-axis shows the lateral dimensions. The y-axis data is the height data. The measurements are taken over the range of 0-1.50mm distance over the entire surface. The profile of the graph shows the surface has peaks and valleys within ± 0.70 µm. The surface profile shows the predominance of the valleys in the surfaces. The formation of the valleys in the surface is due to the vibrations induced in the sample during the lapping process.

3.7 Surface Characterization of Electroplated sample without deterministic microasperities

The lapped surface is coated with a thin layer of the nickel (approximately 5µm) by the electroplating process. The figure shows the surface measurements through the profilometer.

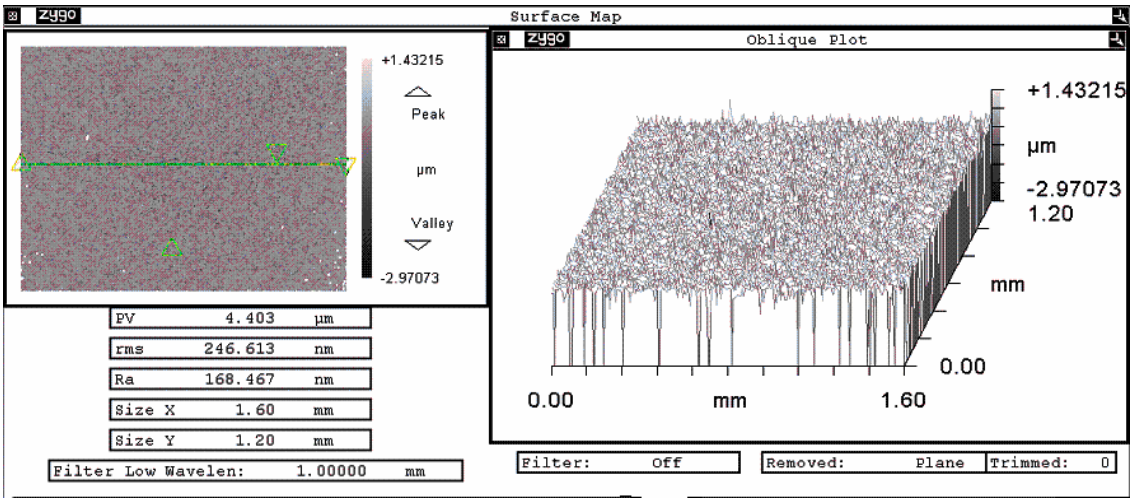

Figure 3.13 Oblique plot of the electroplated sample (*)

The oblique plot in Figure 3.13 shows that the surface has a consistent roughness value the same as that of the lapped sample. The surface profile of lapped samples shows less variation in peaks and valleys as compared to the lapped sample. The average deviation in the peaks and valleys in the surface is approximately within range of 0.10µm in the surface. Proper lapping and plating the sample can minimize the deviation in the surface. The nickel plating provides a good adhesive layer for microasperities.

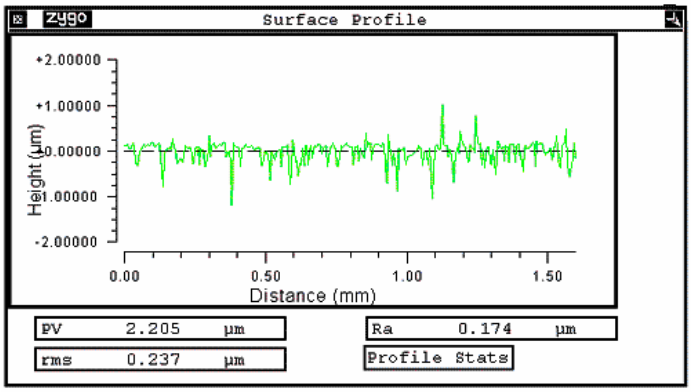

Figure 3.14 Surface profile of the nickel plated sample (*)

3.8 Surface Characterization of Positive Square microasperities

Positive asperities are fabricated using the modified photolithography process of electroplating. The microasperities are characterized using the optical profilometer and using the scanning electron microscope.

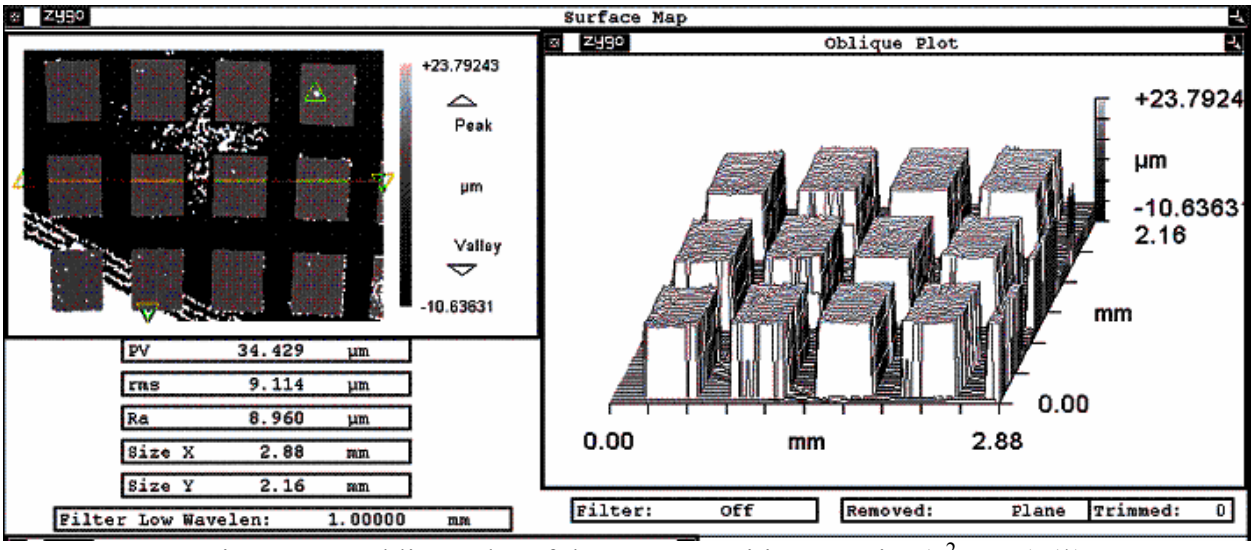

Figure 3.15 Oblique plot of the square positive asperity (δ^2: 0.40) (*)

Figure 3.15 shows the oblique plot of the square asperity (δ^2: 0.40) by using the 3-D optical profilometer. The average roughness on the top of the microasperities is measured and noted. The roughness on the top of the microasperities plays a vital role in the tribological properties such as the coefficient of friction and the wear of the thrust surface. The average dimension of the square asperity is 480x 480 µm and 20 µm tall. The average dimension of the micro asperity increases from the center of the thrust ring to the outer diameter of the ring. The average spacing between the microasperities is approximately 200µm. The average surface roughness (R_a) on the top of the asperity is 9.196µm. The higher the R_a, the better the surface roughness on top of the micro asperity, which helps in increasing the coefficient of friction and helps in increasing the load carrying capacity of the thrust surface. The average root mean square (rms) value of the surface is the root mean square roughness of the surface; the rms value of the surface is approximately the same as the R_a value (i.e. 9.107µm) is over entire surface of the micro asperity. The array of the micro asperity is arranged radially over the entire thrust surface. Lapping the microasperities can control the height of microasperities.

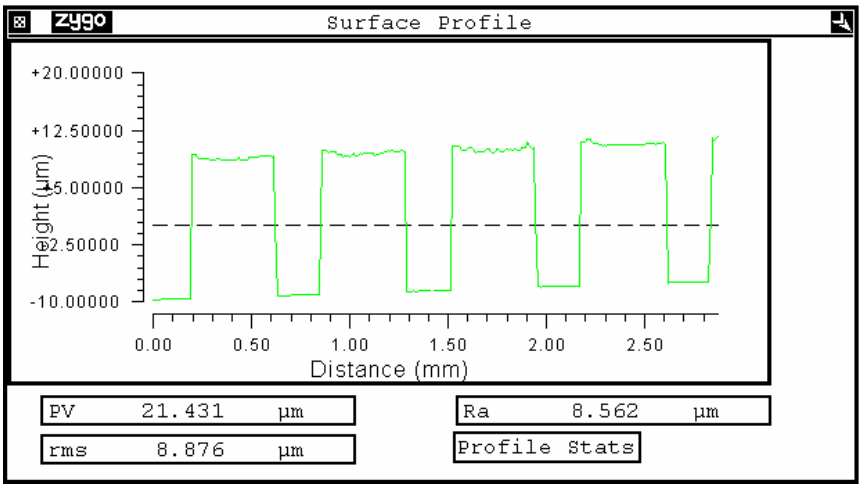

Figure 3.16 Surface profile plot of the square microasperity (δ^2: 0.40) (*)

Figure 3.16 shows the surface profile plot of the square micro asperity. This is a two-dimensional plot, with x-axis showing lateral dimensions and y-axis is showing height data. The data is taken over the length of 2.50mm. The surface profile shows that the microasperities are of the same height and are equidistant from each other. The PV (Peak value) of the surface shows the amount of peaks and valleys in the surface. The higher the PV value, the higher the difference between the peaks and valleys in the surface. The average roughness (R_a) and root mean square (rms) is approximately the same over entire surface. The microasperities are spread uniformly all over the thrust surface and have consistent surface roughness over the entire surface.

3.9 Surface Characterization of Triangular Positive asperities

The triangular asperities of the aspect ratio (δ^2: 0.20) are fabricated using the UV lithography process fabricated at University of Kentucky, which has been discussed in detail in the Chapter 2. The surface characterization is done by using the 3-D Surface profilometer.

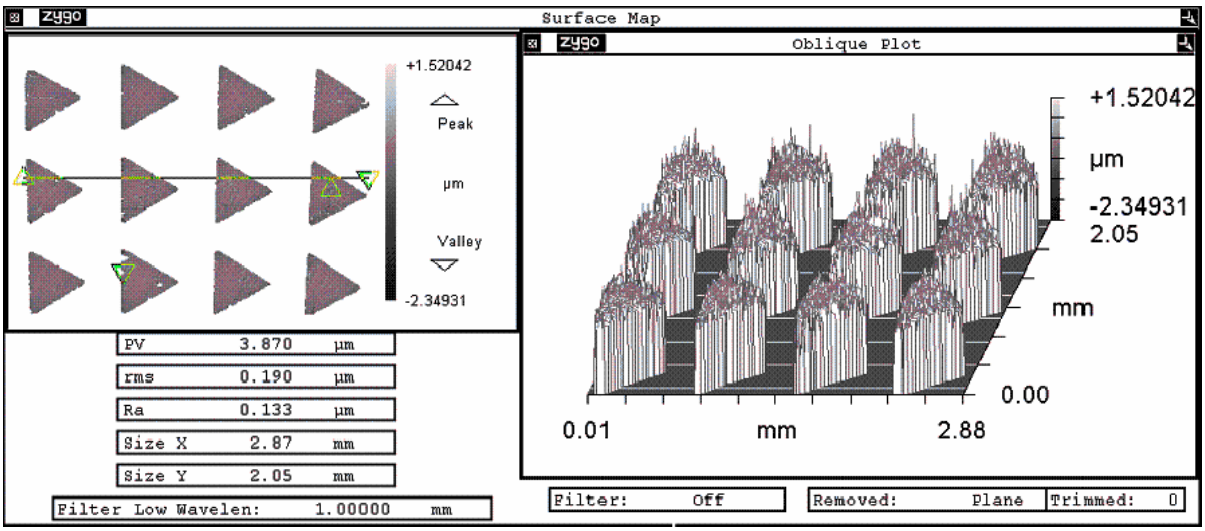

Figure 3.17 Oblique plot of the triangular microasperities (δ^2: 0.20) (#)

Figure 3.17 shows the oblique plot of the triangular microasperity (δ^2: 0.20***)*** using an optical interferometer. The measurements are taken similarly to the square microasperity. The average roughness over entire surface of the microasperity is measured (R_a=0.206 µm). The average roughness indicates the surface has uniform flatness all over the surface. The average root mean square roughness value (rms= 0.148µm) is approximately the same as the R_a value over the entire surface. The average dimensions of the triangular asperity are the sides of the equilateral triangle (Average dimension of each side of triangle is 515 µm, and height of the triangle is 445 µm). The average height of the microasperity is approximately 5µm.

The surface plot given below shows the surface profile plot of the triangular microasperity. The surface profile shows that the triangular asperities are equidistant from each other. The microasperities have equal average height. The PV (peak value) of the surface suggests that the average variation in peaks and valleys of the surface is minimal. The surface is extremely flat and has good load carrying capacity for thrust surfaces.

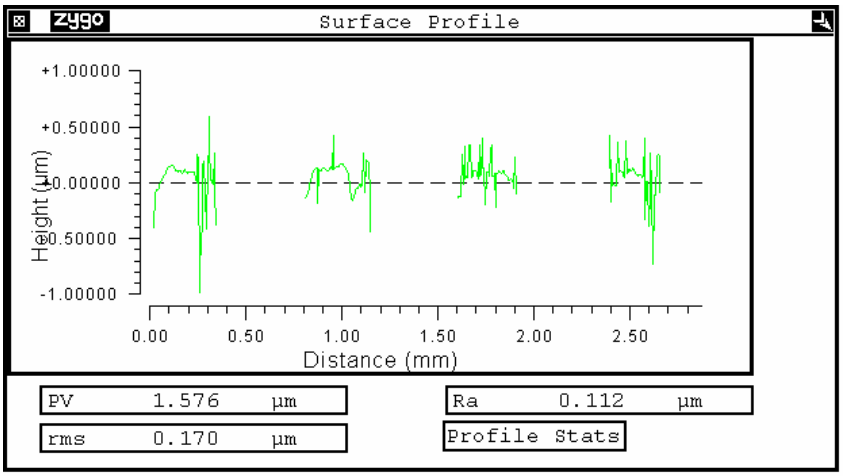

Figure 3.18 Surface plot of triangular microasperities (δ^2: 0.20) (#)

3.10 Surface Characterization of Square Cavities

The cavities have several advantages over the positive asperities. The presence of the negative asperities on the lubricated surface shows a significant improvement in reducing the coefficient of friction and increasing load carrying capacity and dynamic stiffness of the thrust surface and the tribological properties of the thrust surface. Figure 3.20 shows the oblique plot of the square cavities (δ^2= 0.40).

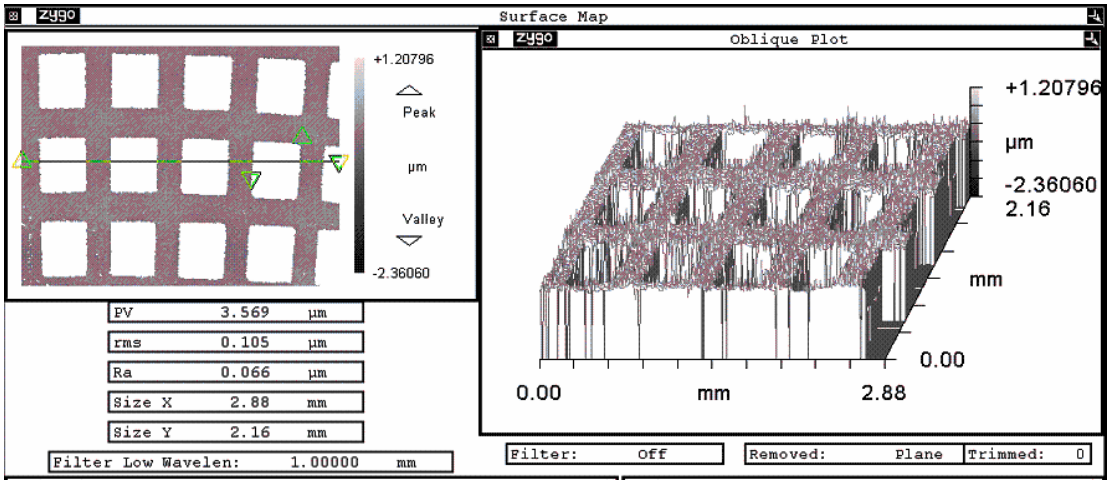

Figure 3.19 Oblique plot of square cavities (δ^2= 0.40)

The average measurement of the surface roughness is noted at the top , within and at the bottom of the microasperity. The average surface roughness value (R_a ≅0.049µm) and the average root mean square roughness is in range of (rms≅ 0.092µm) value. These

values reflect that the surface has uniform flatness and excellent for the tribological applications. The data extracted from the optical profilometer is analyzed by using Matlab to find the skewness and kurtosis of the thrust surface. The skewness is a measure of the asymmetry of the profile about the mean line. The result obtained from the Matlab gives a skewness value of (–0.1110). The negative skewness value shows the predominance of the valleys in the surface, while positive skewness shows the predominance of the peaks in the surface. The skewness is illustrated to carry load carrying capacity and porosity. Negative skewness is a criterion for a good bearing surface.

Figure 3.20 shows the surface profile plot of the negative square asperity. The dimensions of the square asperities are 480x480µm, with the average depth of the microasperity at 25µm. The microasperities are made of nickel. The depth of the microasperities can be controlled by the lapping process. The surface profile shows that the asperities are equidistant and have same depth over the entire surface.

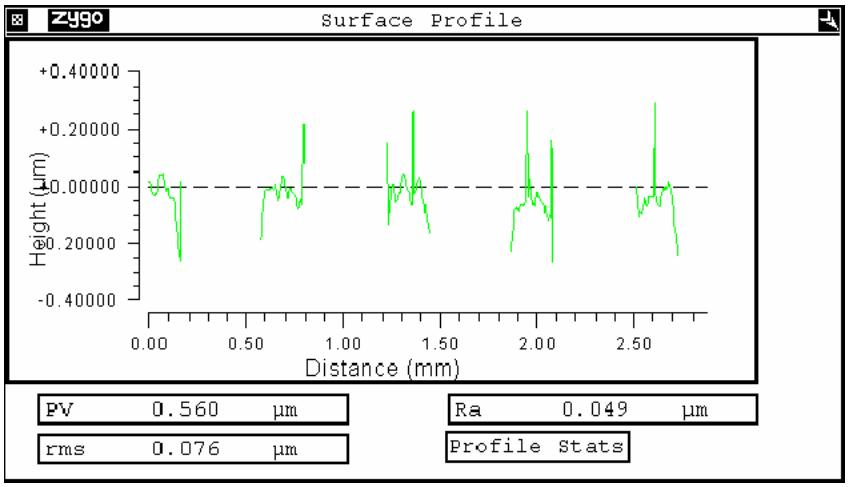

Figure 3.20 Surface profile plot of negative square microasperity (δ^2= 0.40).

3.11 Surface Characterization of Triangular Cavities

The triangular cavities of the aspect ratio (δ^2: 0.20) are fabricated using the UV lithography process fabricated at University of Kentucky, discussed in detail in Chapter 2.The figure shows the oblique plot of the triangular microasperity by using optical profilometer.

The average measurement of the surface roughness is noted at the top, within and at the bottom of the microasperity. The average surface roughness value (R_a ≅0.071µm) and the average root mean square roughness is in the range of (rms≅ 0.156µm) value. These values reflect that the surface has uniform flatness and is excellent for the tribological applications. The data extracted from the optical profilometer is analyzed by using Matlab to find the skewness and kurtosis of the thrust surface. The skewness is a measure of the asymmetry of the profile about the mean line. The result obtained from the Matlab gives a skewness value of (–0.2500). The negative skewness value shows the predominance of the valleys in the surface, while positive skewness shows the predominance of the peaks in the surface. The skewness is illustrated to carry load carrying capacity and porosity. Negative skewness is a criterion for a good bearing surface.

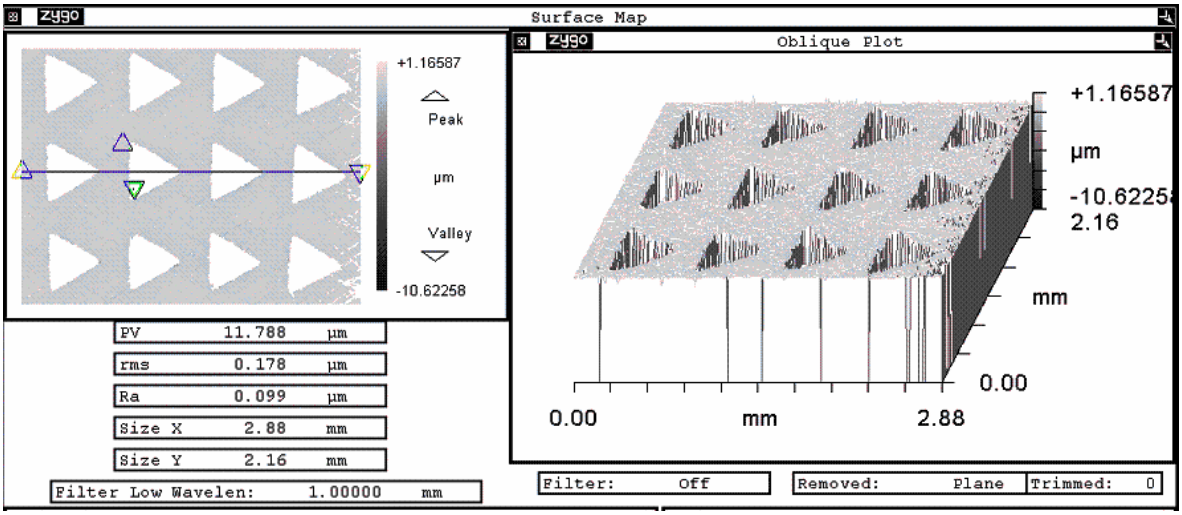

Figure 3.21 Surface profile plot of negative square microasperity (δ2= 0.20).

Figure 3.21 shows, the surface profile plot of the negative square asperity. The dimensions of the triangular asperities are 525µm sides, 450µm height, and the average

depth of the microasperity is 10μm. The microasperities are made of nickel. The depth of the microasperities can be controlled by the lapping process. The surface profile shows that the asperities are equidistant and have same depth over the entire surface.

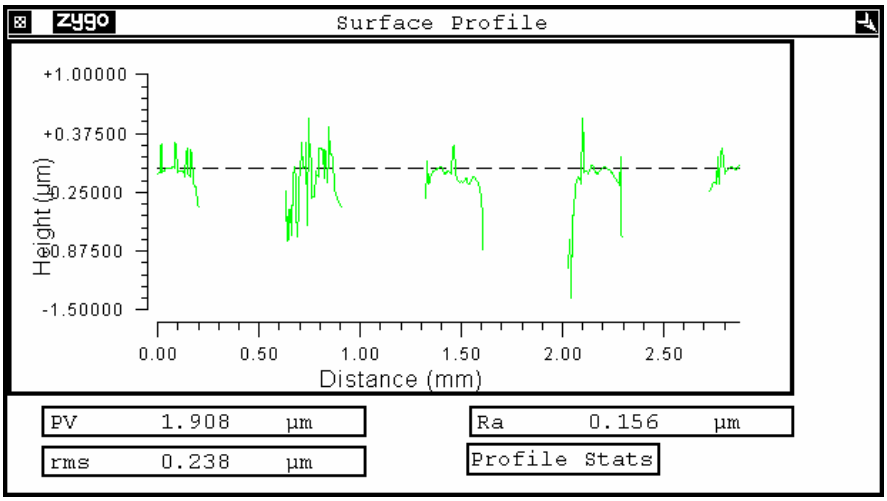

Figure 3.22 Surface plot of negative square microasperity (δ2= 0.20).

3.12 Electron Microscopy

The scanning electron microscope [20] generates a beam of electrons in a vacuum. That beam is collimated by electromagnetic condenser lenses, focused by an objective lens, and scanned across the surface of the sample by electromagnetic deflection coils. The primary imaging method is by collecting secondary electrons that are released by the sample. The secondary electrons are detected by a scintillation material that produces flashes of light from the electrons. The light flashes are then detected and amplified by a photomultiplier tube. By correlating the sample scan position with the resulting signal, an image can be formed that is strikingly similar to what would be seen through an optical microscope. The illumination and shadowing show a quite natural looking surface topography.

Backscatter imaging uses high-energy electrons that emerge nearly 180 degrees from the illuminating beam direction. The backscatter electron yield is a function of the

average atomic number of each point on the sample, and thus can give compositional information.

3.12.1 Working Principle of Scanning Electron Microscope

A beam of high-energy electrons is produced in the electron gun at the top of the column by applying high voltage to a tungsten filament and nearby anode. This beam is accelerated down past the anode into the column where it is condensed and aligned by a series of electromagnetic lenses and coils within the column. This focused beam continuously rasters back and forth across the sample. Interactions between the electron beam and the sample result in the emission of different types of energies that are measured by a series of detectors within the sample chambers. The four types of emissions that are measured are: Secondary electrons, Backscattered electrons, x-rays and the cathode luminescence. X-ray data is sent to the EDS where it is translated into elemental plots. The other three detectors are connected to a 'TV' screen where the signal produces a clear, black and white (green actually) image of the sample. Secondary electron imaging provides a good 3-dimensional topographic view of the sample. Backscattered electron images show less defined topography but they clearly display difference in the elemental compositions because higher elements higher in atomic number appear brighter. Cathode luminescence imaging highlights chemical variations within individual grains due to trace element variations and zoning.

The electron microscopy is used to study the intricate details of the microasperity. The surface profile has limitation of lateral resolution and Scanning electron microscope offers highest resolution in range of few nanometers. The edge of microasperities, square array of the microasperity and also height of microasperity (thickness) can be easily seen through scanning electron microscope. The defects within the microasperities and surface roughness (nickel grains) can be observed by using scanning electron microscope.

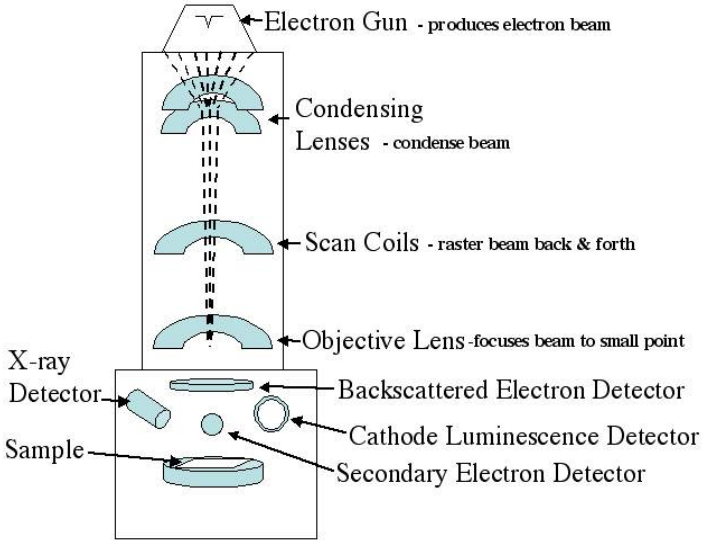

Figure 3.23 Schematic diagram of working of Scanning Electron Microscope

3.13 Images taken from Scanning Electron Microscope

3.13.1 Square Microasperity

Figure 3.24 shows the SEM image of a single square asperity ($\delta^{2:}$ 0.40) obtained by using the backscatter detector in order to avoid the charging issues during microscopy. The average dimension of the square microasperity is 480x480μm and the average height of the microasperity is about 15μm.

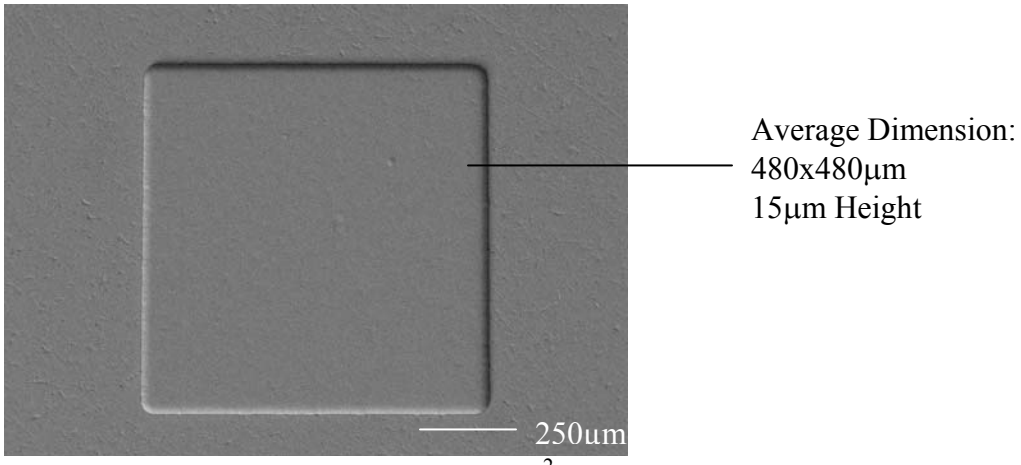

Figure 3.24 Single square microasperity (δ^2 : 0.40)

Figure 3.25 shows a SEM image of the square microasperity ($\delta^{2:}$ 0.40) without using a backscatter detector. The lapping marks on the substrate can be clearly observed

along with the charging of the electrons at the edge of the microasperity. The charging issues during measurement can be avoided by using the backscatter detector.

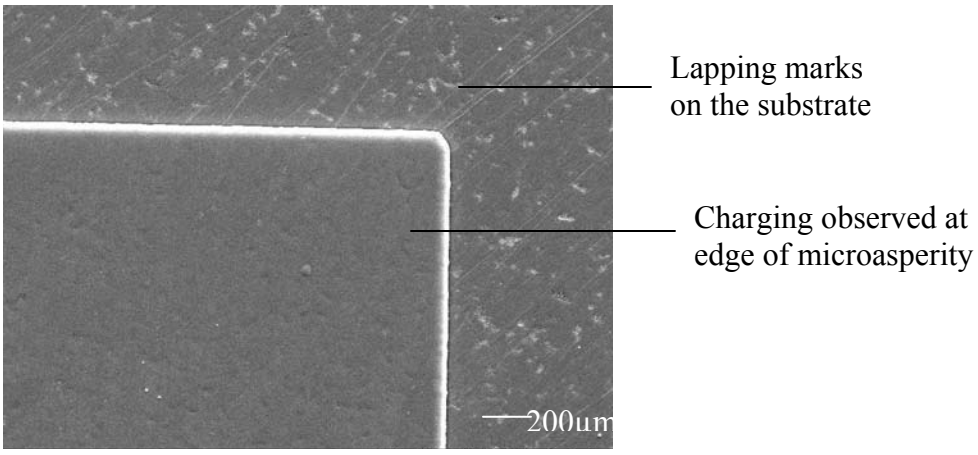

Figure 3.25 Edge of the square microasperity

Figure 3.26 shows the straightness error at the edge of the square microasperity. The edge of the microasperity is magnified in order to calculate the straight edge error. The error might have occurred due to the limitation of the resolution of the UV lithography process. The error in the edge of the microasperity is within 20µm.

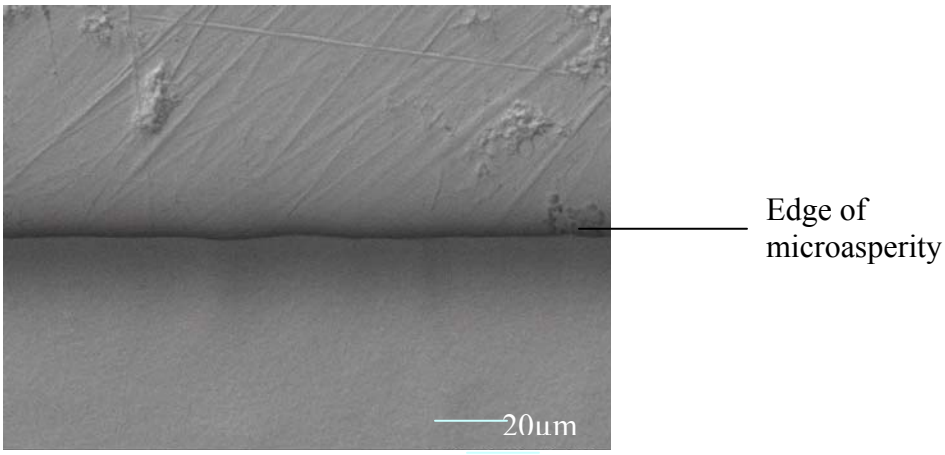

Figure 3.26 Straightness error in the edge of square microasperity

Figure 3.27 shows the edge of the square microasperity. The edge of the square asperity shows a radial curvature at its tip. The radial curvature might have occurred due to the process variation and exposure dose. The sample is tilted at 80° and focused on the edge of the sample to observe the thickness of the microasperities. The average thickness of the microasperities observed in this figure is approximately 15µm.

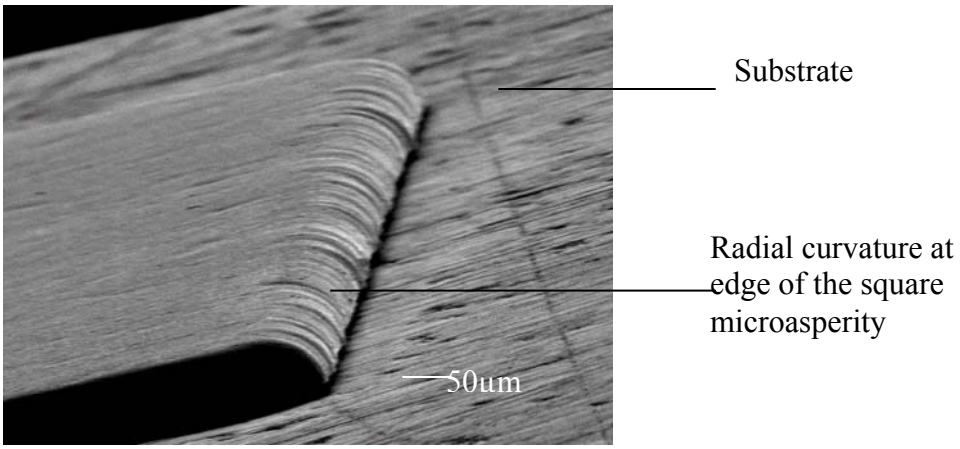

Figure 3.27 Height of square microasperity

Figure 3.28 shows an array of the square positive asperities arranged radially on the thrust surface. The microasperities have uniform thickness and slight radial curvature at the tip of the microasperities.

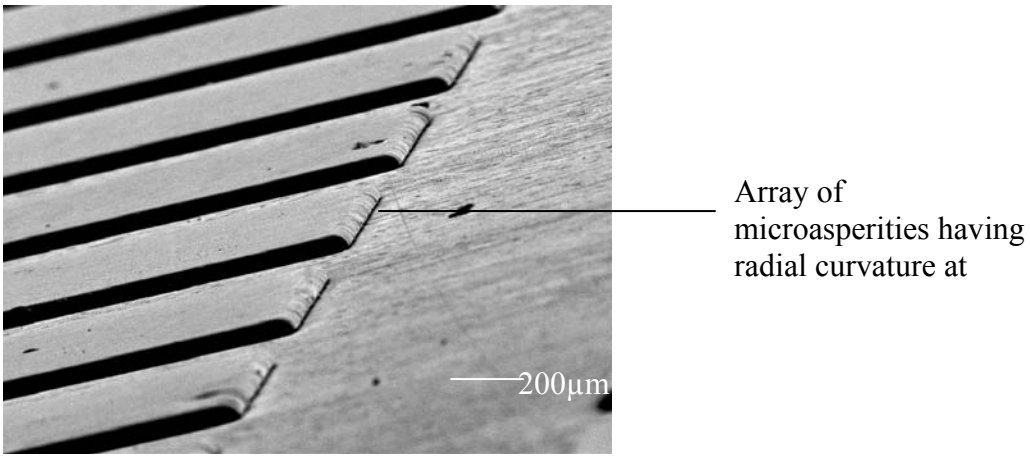

Figure 3.28 Array of positive square microasperities (δ^2=0.40)

3.13.2 Triangular microasperity

Figure 3.29 shows the SEM image of the triangular positive microasperity having the area- fraction ratio of (δ^2=0.20) using the backscatter detector. The triangular micro-asperity is an equilateral triangle having the average dimension (side of triangle is 515µm) and average height of the triangle is 445µm. The average height of the post is 15µm.

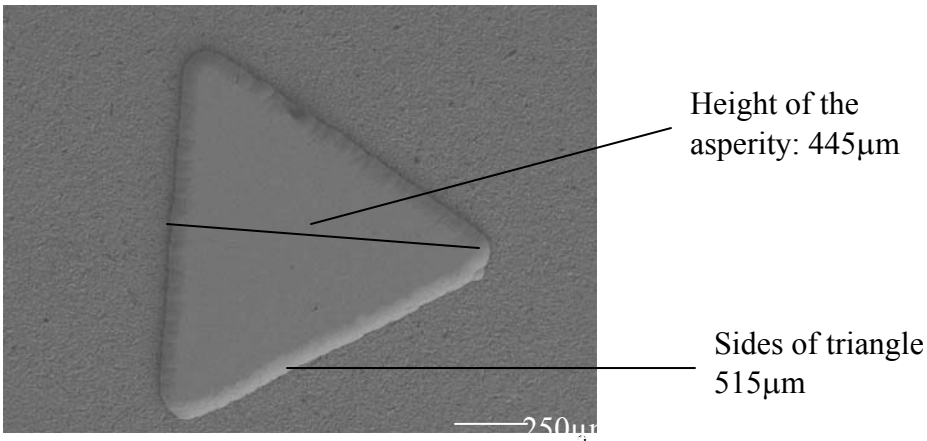

Figure 3.29 Triangular positive microasperity (δ^2= 0.20)

Figure 3.30 shows the edge of the triangle of positive triangular microasperity (δ^2: 0.20). The average deviation in the dimension of the triangular microasperities is noted. The deviation in dimension is due to process limitation, especially exposure dose and exposure time, which makes a significant impact on the overall dimensions of the microasperity.

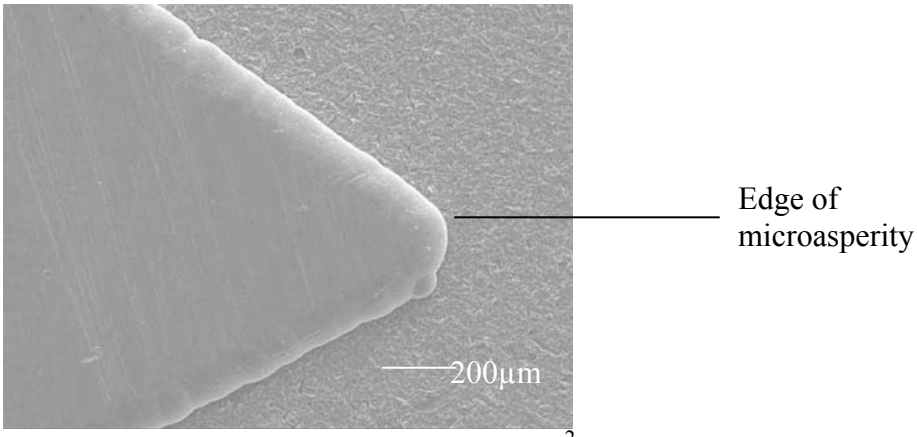

Figure 3.30 Triangular positive microasperities (δ^2: 0.20) with an edge

The deterministic microasperities characterized using the Optical interferometer and scanning electron microscope. The various surface parameter such average surface roughness, root mean square value, peak value, skewness and kurtosis of the surface is measured. The dimensions of the deterministic microasperities are measured using the optical microscope.

The fabricated deterministic microasperities are carefully characterized by using the precise instrument such as optical interferometer, optical microscope and scanning

electron microscope. The various surface parameters such as average roughness, root mean square value, peak value, skewness and kurtosis of the are measured using 3-D surface profilometer. These surface parameters are studied during entire fabrication process. These surface parameter plays significant role in tribological properties of thrust surface.

The average dimension of the fabricated microasperities is compared with dimension of photomask. The average variation in the dimension is in the range of 5-7μm.

CHAPTER 4 - NOVEL ALIGNEMENT TECHNIQUE

4.1 Introduction

We have discussed in Chapter 2 the detailed manufacturing process to fabricate deterministic microasperities on the thrust surface. Substrate flatness, photoresist thickness, exposure dose, pre-baking conditions and post exposure baking, along with developing time, are the important process parameters in the manufacturing of deterministic microasperities. Apart from these processing parameters, accuracy and repeatability of patterns produced are also important parameters in the overall manufacturing process. The shape, size and orientation of the microasperities depend on the type of patterns engraved in the photomask. The patterns engraved on the photomask have accuracy within 2-3 microns radially as well as longitudinally.

The typical layer diagram of the photomask is shown in the Figure 4.1a. The typical photomask is 4"x 4" in size and is made of soda lime glass coated with a thin layer of chromium oxide, which minimizes the wear of the patterns during direct contact exposure in the photolithography process. The patterns are arranged radially in the photomask.

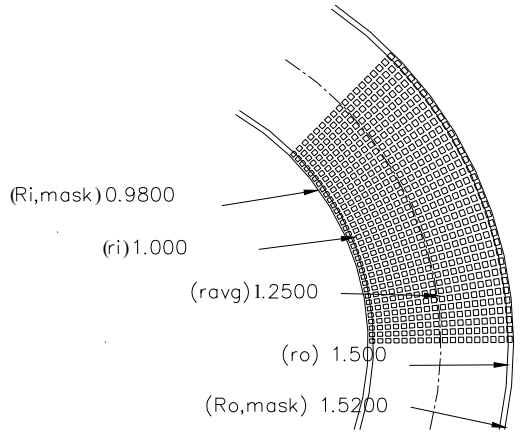

Figure 4.1a Layer diagram of square photomask

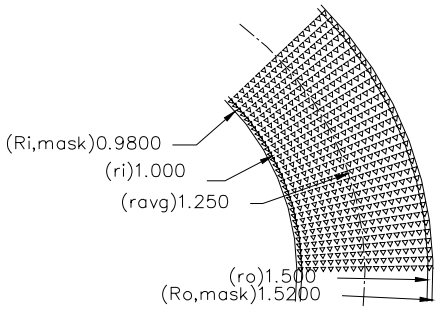

Figure 4.1b Layer diagram of photomask (δ^2 =0.20)

The specific shape, size, and orientation of the pattern are obtained from the analytical model generated by solving the Reynolds equation. The patterns are radially symmetric about the Ravg (average radius of ring). Typically there are 9 unit cells above and below the Ravg. The size of the unit cell increases from center of the mask to the outer edge of the photomask. Each unit cell has patterns engraved on it.

Since the patterns are arranged radially and are not spread over the entire photomask, it is difficult to get accurate and aligned patterns on the substrate. The exact dimension and alignment of the patterns are essential for tribological studies such as wear, load carrying capacity, and the coefficient of friction of thrust surfaces.

4.2 Novel Alignment Technique

The Novel alignment technique developed at Bearing and Seals Laboratory at University of Kentucky has been used to produce accurate and repeatable patterns**.** The Novel alignment technique is a simple and extremely accurate method of producing accurate and repeatable patterns. Alignment marks are made on the photomask and the substrate using Electrical Discharge Machining (EDM). During the actual exposure, the alignment mark (cross mark) on the photomask is focused by the microscopic lens

attached to the mask aligner. The position of the microscope is kept fixed, and the alignment mark on the substrate is later focused by adjusting the motion of the stage of the mask aligner in "x" and "y" direction. Thus, the alignment of the photomask and the substrate is done individually. The accuracy of the patterns also depends on the actual motion of the stage during alignment, as well as on the contact of the substrate with the photomask. The magnification used in focusing the alignment marks also makes a significant difference in the alignment.

The alignment marks made on the substrate and the photomask are cross marks (holes) of 50 microns in diameter, 7 microns deep and equidistant by 250 micron. The accuracy of the holes drilled by using EDM depends on the edge of the substrate.

4.3 Working Principle Of Micro EDM

The working principle of EDM is very simple. During the process a conductive tool (tungsten) cathode and the substrate (stainless steel) anode are connected to an RC circuit [13]. As the tool electrode approaches the substrate, impedance between the two becomes greater than the impedance in the capacitor. At this point discharge occurs, resulting in a plasma column between the two objects. The working principle is shown in Figure 4.2.

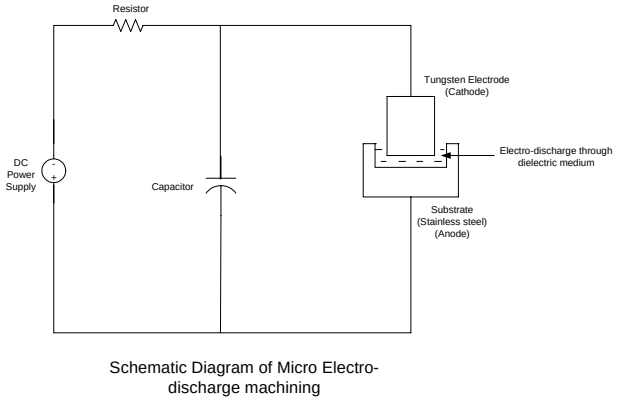

Figure 4.2 Schematic diagram of working of Micro EDM

The flux of electrons causes the cathode and the anode to heat up above their melting temperatures. The voltage supply is pulsing with a bandwidth of approximately 500ns; therefore when the pulse closes, the plasma column collapses and melted

materials become particulate. The discharge occurs across a small gap (~2μm) filled with dielectric oil, which increases impedance and assists in flushing the particulate out of the gap. As the pulse continues, more material is removed from cathode and anode, replicating the shape of the tool electrode into the substrate.

Figure 4.3 shows the actual machining setup of the process, the tungsten electrode and the substrate (stainless steel). The tungsten tip is grounded on an EDM machine to get the desired diameter of the tip of the electrode, which is 50μm.

Figure 4.3 Actual machining setup

Figure 4.4 shows the actual machining process. The electrode is in contact with the substrate during the machining process. The substrate is positioned with respect to the tungsten electrode. The depth of the cut can be controlled through the position of the "z" axis of the electrode. The average depth of the hole is in the range of 8-8.5μm. The processing time is approximately 1 minute.

Figure 4.4 Actual EDM machining process

4.4 Alignment Marks

Figure 4.5 shows cross hairs made on the substrate using the EDM process. Initially the center of the substrate is found precisely by focusing the microscopes. The program was written so that it would control the movement of the electrode. Diameter and distance between the holes are controlled by executing the program.

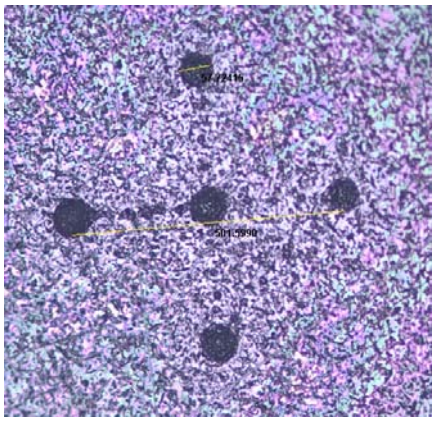

Figure 4.5 Cross hairs on substrate

Figure 4.6 shows the cross hairs made on the photomask. The average dimension of the hole is 57.7215μm. The diametrical distance between the holes is 501.60μm. The accuracy of the holes produced is within nanometers. The cross heirs on the photomask and substrate are taken as reference for accurate alignment of the photomask and the substrate.

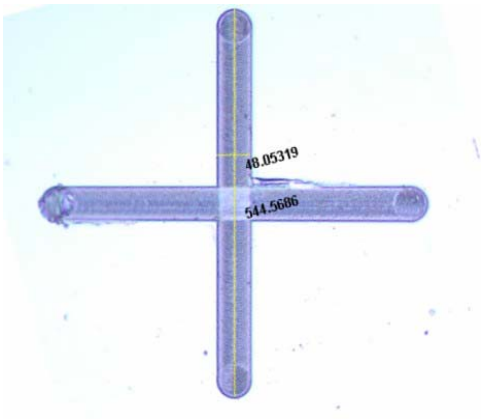

Figure 4.6 Cross hairs on photomask

Figure 4.7 shows the result of the pattern generated using the novel alignment method described above. The average radial and circumferential dimensions between the patterns are noted and it was observed that patterns are radially symmetrical within 20 μm. The novel alignment technique is a simple and extremely accurate process. The results obtained using alignments are extremely accurate. Making alignment marks on the substrate and photomask can easily solve the problem of eccentricity. The results shown through this process are remarkably accurate.

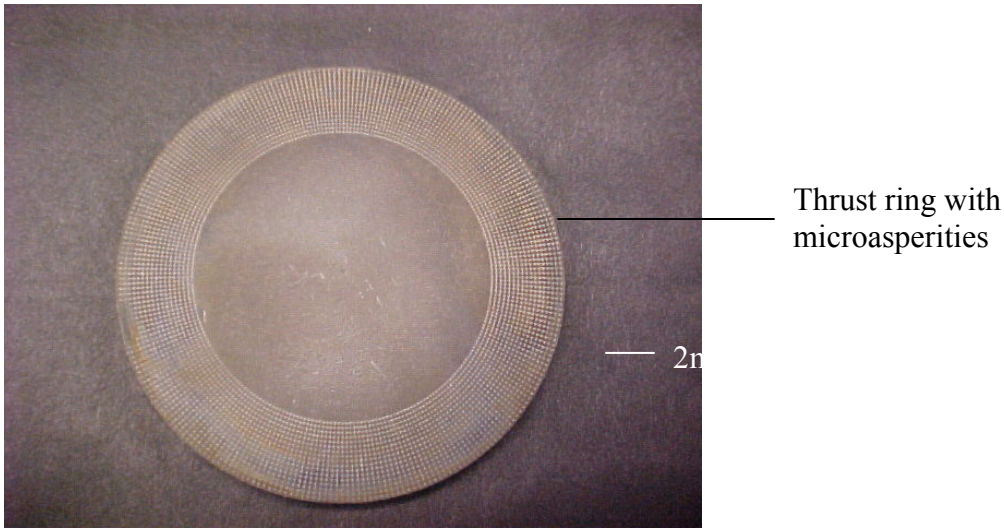

Figure 4.7 Aligned patterns after Novel Alignment Technique

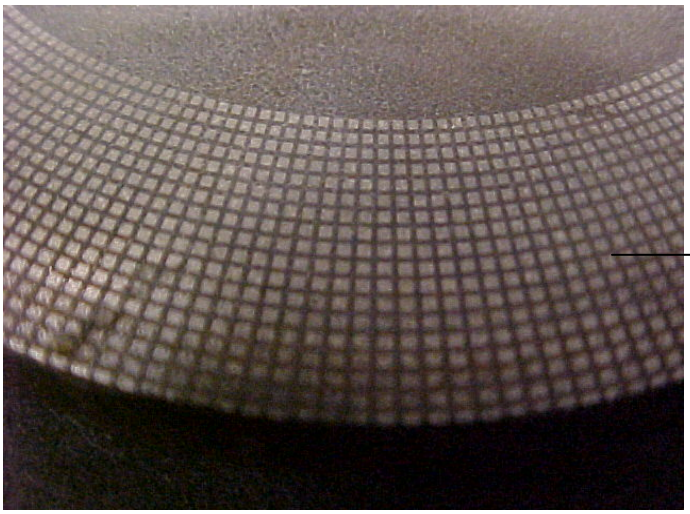

Figure 4.8 Square aligned patterns (radially arranged)

The above optical microscope image (Figure 4.8) shows the alignment of square patterns. The photomask and substrate aligned using Novel alignment technique. The process has remarkably pattern and shows very accurate and repeatable patterns. The average deviation (radially and horizontally) measured is within the accuracy of 10-15microns.

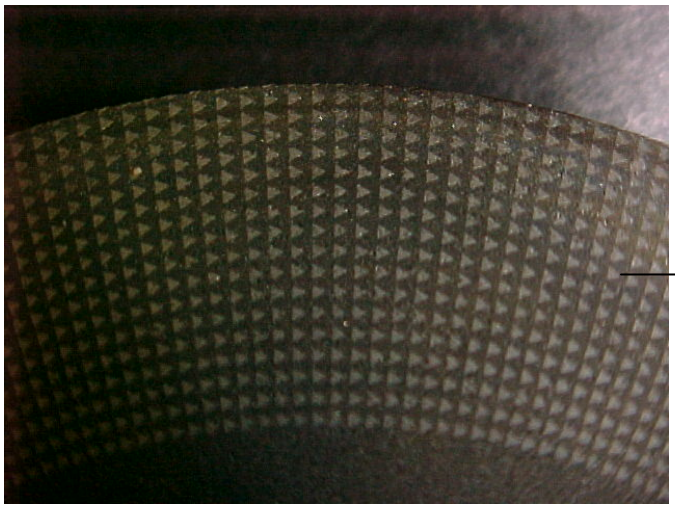

Figure 4.9 Triangular aligned patterns (radially arranged)

The figure 4.9 shows the triangular microasperities (nickel) arranged radially on the thrust surface. The novel alignment technique shows remarkable improvement in the alignment of the patterns. The patterns are extremely accurate and repetable in nature. The average deviation in the measurement of the pattern is within range of 10microns accuracy.

4.5 Limitation of Novel Alignment Technique

The novel alignment technique is a simple, accurate and extremely useful method for mass-producing deterministic microasperities. The results obtained by using this process are repeatable and accurate; however, there are certain limitations in the existing process. The effectiveness of the alignment process depends on the accuracy of alignment marks made by using the EDM machine. Each substrate has a different edge reference, so every time we have to find perfect edge of the substrate and set the machine to zero. Whenever, we need to take same reference for the “x” and “z” co-ordinates, we have to make some minor adjustments.

The cost of machining one part of stainless steel substrate is very high. The EDM machine has very high machine hour rate (Approximately $500 per/hr), so it is not economical to use this process for low cost high production manufacturing. Moreover skilled and trained personnel are required to operate the EDM. The setup cost and tools required for machining makes the process extremely difficult for mass production.

CHAPTER 5 - CONCLUSION, DISCUSSION AND FUTURE WORK

5.1 Conclusion

A fabrication process was developed for fabricating deterministic microasperities on a thrust surface at Bearing and Seals Laboratory, University of Kentucky. This process is extremely useful for fabricating both positive and negative microasperities having low a aspect ratio.

1) The fabrication process developed manufactures the deterministic positive and negative microasperities on thrust surface successfully.
2) The process is extremely useful for mass production of microasperities and shows remarkably accurate and repeatable patterns in radial direction.
3) Any arbitrary shape, size, and orientation of the microasperities can be fabricated using the above process.
4) The process developed at University of Kentucky is used to fabricate both positive as well as negative asperities, unlike the laser texturing process, which fabricates only negative asperities.
5) Surface characterization using the optical interferometer and scanning electron microscope shows the surface variation on top, within, and at the bottom of microasperities.
6) The Novel alignment technique is a simple yet extremely accurate process for producing radially accurate patterns. Accuracy of patterns generated is within 20μm (radially).
7) Unlike the modified LIGA process, in which a template is fully utilized (consumed), wear of the photomask is negligible in this case, and the template can be reused for many times.
8) The accuracy of the microasperities depends on various process parameters such as substrate flatness, photoresist coating, alignment and baking. All parameters should be critically controlled in order to get uniform and aligned patterns.

5.2 Discussion

The fabrication process developed at Bearing and Seals Laboratory, University of Kentucky is useful for fabricating positive as well as negative microasperities on thrust surfaces. The process is extremely useful for manufacturing low aspect ratio microstructures. The quality of patterns produced by this process depends on many of process parameters discussed in this section.

The thrust surface (stainless steel ring) on which microasperities is to be fabricated should be a flat surface. The surface should be lapped within 2-3 light bands. Flatness of the surface is important to get a uniform nickel coating on top of the substrate. Adhesion of the nickel asperities on the thrust surface depends on the quality of the thin layer of nickel deposited on the thrust surface. The electroplating process should be carried out at a constant voltage (i.e.Galvanostatic mode). The amount of current density applied across the circuit depends on the surface area to be plated. The plating rate and amount of current density applied depends on the thickness of the plating required. The solution concentration, the pH of the solution, and the temperature of the water bath play vital role in the quality of electroplating.

After the thrust sample is plated with nickel, the sample is spin coated with the photoresist. The spinning process is of primary importance to ensure the pattern transfer. The quality of the resist coating determines the density of defects transferred to the device. The coating thickness of the thin, glassy resist film depends on the chemical resistance required for the image transfer and the fineness of the lines and the spaces to be resolved. The application of too much resist results in edge covering or run-out, hillocks, and ridges, thus reducing manufacturing yield. Too little resist may leave uncovered area. Optimization of the “regular” photoresist coating process in terms of resist dispense rate, dispense volume, spin speed, ambient temperature, and humidity presents a growing challenge in micro-electronic industry. An on-line film thickness monitor, possibly a technique based on reflection spectroscopy, will become essential for statistical process control for photoresist coating.

After spinning, the resist still contains 15% solvent and may contain built- in stress. Baking time should be optimized for proximity and conventional hot plates, since

solvent evaporation rate is influenced by the rate of heat transfer. For better results, an initial lower soft bake temperature allows the solvent to evaporate out of the film at a more controlled rate, which results in better coating fidelity, reducing the edge bead as well as better resist- substrate adhesion.

After soft baking, the resist coating substrate is transferred to an exposure system; photomask is aligned with the features on the mask. The alignment of the Photomask and the substrate is discussed in detail in Chapter 4. The purpose of the illumination is to deliver light with the proper intensity, directionality, spectral characteristics, and uniformly across the substrate, allowing a nearly perfect transfer or printing of the mask image in the form of latent image. SU8 is optimized for near UV (350nm-400nm) exposure. SU8 is virtually transparent and insensitive above 400nm but has high actinic absorption below 350nm. An excessive dose below 350nm results in the over exposure of the top portion of the resist film, resulting in exaggerated negative sidewall or "T" topping. The optimum exposure dose depends on film thickness and exposure parameters.

Post exposure treatment must be performed to cross link the exposed portion of the film. Optimum cross-link density is obtained through careful adjustments of the exposure and PEB conditions. SU-8 is readily cross-linked and can results in highly stressed film. To minimize the stresses, substrate bowing and resist cracking a slow ramp down are recommended. Rapid cooling after post exposure bake should be avoided.

Strong agitation is required for high aspect ratio and for thick film structures. The dissolution rates can vary widely as a function of the agitation rate, temperature, and resist processing parameters.

Etching of the photo-resist is the most difficult step of the entire process. For positive photoresist, heating the substrate in boiling acetone at 120°C for 3-4 minutes results in complete etching. SU8 is extremely difficult to etch. The substrate coated with SU8 is kept in oven maintained at a temperature of 450- 500°C for 4-5 hours. Excessive heating induces thermal stresses on the substrate, while if heated for lesser time, the photoresist remains on the substrate.

Process parameters, which affect the quality of the deterministic microasperities produced by fabricating process are discussed above.

5.3 Future Work

Deterministic microasperities are fabricated on the thrust surface successfully by using the method proposed in this thesis. The process is suitable for fabricating positive and negative microasperities. In future, the process should be optimized for commercial mass production.

a) Fabrication process should be optimized for commercial mass production

b) Process should be modified to fabricate the deterministic microasperities on the circumference of the thrust surface.

c) Effort of the surface roughness of the substrate should be studied in detail.

d) Deterministic microasperities should be fabricated on the different materials such as Ceramics, polymers, rubber and other alloys.

e) Process variation should be quantified during the process and statistical method should be used to check the accuracy of the process.

REFERENCES

1. Hamilton, D.B., Walowit, J.A., & Allen, C.M., "A Theory of Lubrication by Microirregularities", Journal of Basic Engineering, Trans ASME, Ser.D; March 1966, pp 177-185.

2. Anno, J.N., Walowit, J.A., & Allen, C.M., "Microasperity Lubrication", Journal of Lubrication Technology, Trans ASME, Ser.F; April 1968, pp351-355.

3. Anno, J.N., Walowit, J.A., & Allen, C.M., "Load Support and Leakage from Microasperity Lubricated Face Seals", Journal of Lubrication Technology, Trans ASME, Ser.F; October 1969, pp 726-731.

4. Etsion, I., Kligerman, Y., & Halperin, G., "Analytical and Experimental Investigation of Laser Textured Mechanical Seal Faces", Tribology Transactions, 42 (3) 1999, pp 511-516.

5. G.RYK., Kligerman, Y., & Etsion, I., "Experimental Investigation of Laser Surface Texturing for Reciprocating Automotive Components", Tribology Transactions, 45(4) 2002, pp 444-449.

6. Stephens, L., Siripuram, R., Hayden, M., & Mccartt, B., "Deterministic Microasperities on Bearings and Seals Using a Modified LIGA Process," ASME/IGTI Conference, Amsterdam, June 2002.

7. Zhang, J., "LIGA Mold Insert fabrication using SU8 photoresist", MS Thesis, Louisiana State University, Dec 2002.

8. Ronen, A., Etsion, I., & Kilgerman, Y., "Friction Reducing Surface Texturing in Reciprocating Automotive Components", Tribology Transactions, 44(3), 2001, pp 359-366.

9. Kortikar, S., Stephens S., Siripuram R., Hadinatha, P., "Manufacturing of Microasperities on Thrust Surface using Ultra- Violet Photolithography Process", American Society of Precision Engineering, Winter Tropical Meeting Jan 2002, pp 146-153.

10. Siripuram, R; Stephens S; "Effect of Deterministic Asperity Geometry on Hydrodynamic Lubrication", Proceedings of 2003 STLE/ASME Joint International Tribology Conference, 2003-TRIB-034.

11. Lapmaster International Manual, IL,USA

12. Bhushan, B; "Modern Tribology Handbook", CRC Press, Volume-I, 2001.

13. Morgan Chris, "Micro Electro Discharge Machining: Techniques and Procedures for Micro Fabrication, MS Thesis, University of Kentucky, May 2004.

14. Zygo Corporation Metropro Manual, Middlefield, CT, USA

15. Patir N., "Effect of surface roughness on partial film lubrication using an average flow model based on numerical solution", PhD Thesis, Northwestern University, Evanston, IL, 1978.

VITA

Author was born in Ahmednagar, India in 1976. He graduated from H.D. High school and attended Walchand Institute of Technology (WIT), Solapur. He completed his Bachelors of Engineering in Production Engineering in 1997, before coming to the United States for attending graduate program in Mechanical Engineering at the University of Kentucky. As a undergraduate he participated in various cultural and sports activities during his undergraduate studies. As a graduate student, he serve as Research assistant in “Bearing and Seals Laboratory” at University of Kentucky. He also presented his research work in national conference ASPE (American Society of Precision Engineering) at Gainesville, FL.